POLITECNICO DI TORINO
Repository ISTITUZIONALE

Hydrogen Sulphide and Carbonyl Sulphide Removal from Biogas for Exploitation in High-Temperature Fuel Cells

Original
Hydrogen Sulphide and Carbonyl Sulphide Removal from Biogas for Exploitation in High-Temperature Fuel Cells / Santoni, F., Gislon, P., Rozzi, E., Gandiglio, M., Mcphail, S., Lanzini, A., Pagani, M., Fiorilli, S.. - In: WASTE AND BIOMASS VALORIZATION. - ISSN 1877-2641. - ELETTRONICO. - 15:(2024), pp. 577-597. [10.1007/s12649-023-02212-6]

Availability:
This version is available at: 11583/2980656 since: 2023-07-25T09:51:40Z

Publisher:
Springer

Published
DOI:10.1007/s12649-023-02212-6

Terms of use:

This article is made available under terms and conditions as specified in the corresponding bibliographic description in the repository

Publisher copyright

(Article begins on next page)

18 November 2026

Waste and Biomass Valorization (2024) 15:577–597
https://doi.org/10.1007/s12649-023-02212-6

ORIGINAL PAPER

Hydrogen Sulphide and Carbonyl Sulphide Removal from Biogas for Exploitation in High-Temperature Fuel Cells

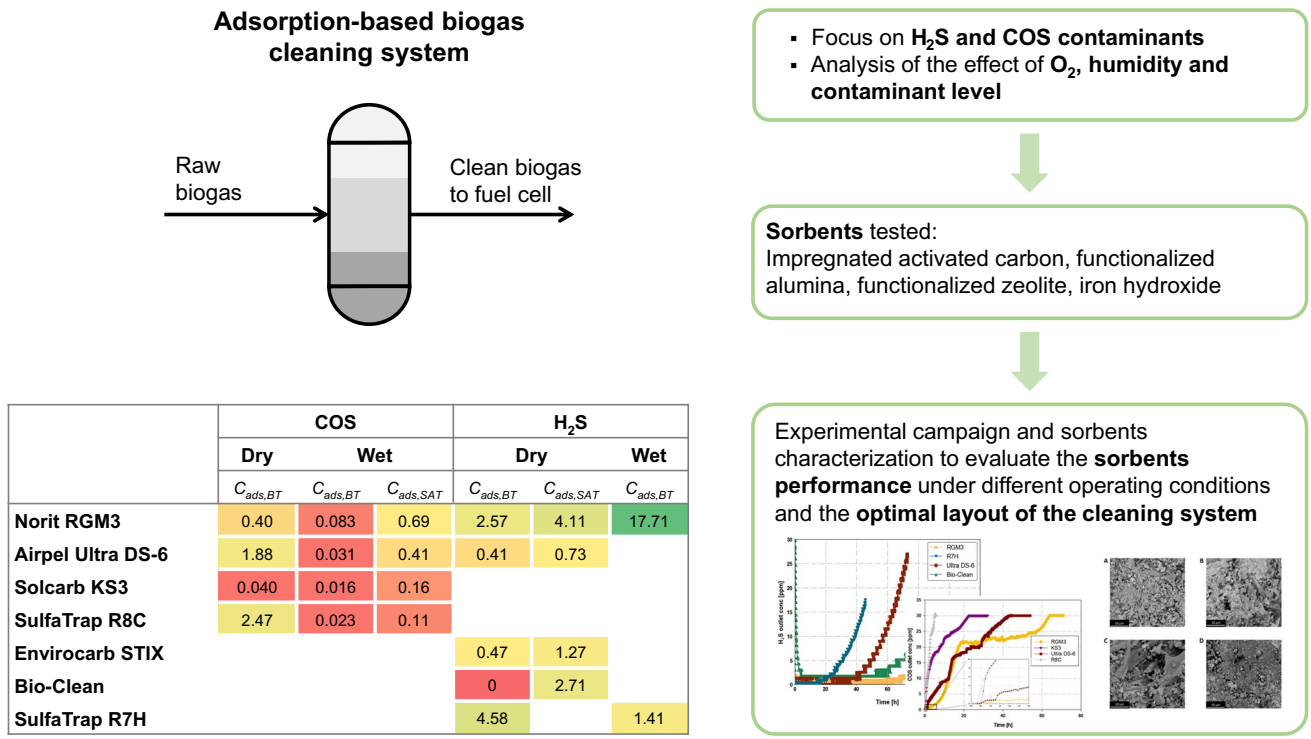
F. Santoni[1] · P. Gislon[1] · E. Rozzi[2] · M. Gandiglio[2] · S. McPhail[1] · A. Lanzini[2] · M. Pagani[3] · S. Fiorilli[3]

Received: 13 February 2023 / Accepted: 14 June 2023 / Published online: 6 July 2023
© The Author(s) 2023

Abstract

Fuel cells powered by biogas for decentralised cogeneration of heat and power are an attractive alternative to combustion technologies. However, biogas contains sulfur-based compounds (H_2S, COS, DMS, siloxanes), which are harmful to fuel cells. This work was carried out in the framework of the European project Waste2Watts, involving the laboratories of Politecnico di Torino, ENEA, and PSI. The aim is to design and test a flexible and cost-effective cleaning unit to remove impurities for the use of biogas in high-efficiency fuel cell systems. The focus is on small- to medium-sized farms for which deep cleaning of biogas by adsorption materials is a suitable techno-economic solution to avoid intensive gas processing treatments. The ability of commercial adsorption materials (activated carbons, metal oxides, and metal hydroxides) to remove hydrogen sulphide and carbonyl sulphide was tested under different biogas compositions (oxygen and humidity). After evaluating the results, three plant configurations were proposed to optimally utilise the potential of the sorbents. Indeed, the RGM3 sorbent has proven to be an effective solution for removing H_2S and COS under humid conditions (50% RH), whilst R7H and R8C sorbents are better suited for removing H_2S and COS, respectively, in dry biogas conditions.

Graphical abstract



	COS			H_2S		
	Dry	Wet		Dry		Wet
	$C_{ads,BT}$	$C_{ads,BT}$	$C_{ads,SAT}$	$C_{ads,BT}$	$C_{ads,SAT}$	$C_{ads,BT}$
Norit RGM3	0.40	0.083	0.69	2.57	4.11	17.71
Airpel Ultra DS-6	1.88	0.031	0.41	0.41	0.73	
Solcarb KS3	0.040	0.016	0.16			
SulfaTrap R8C	2.47	0.023	0.11			
Envirocarb STIX				0.47	1.27	
Bio-Clean				0	2.71	
SulfaTrap R7H				4.58		1.41

Keywords Agricultural wastes · Biogas · Biogas cleaning · SOFC · Activated carbon · Sulphur contaminants

Extended author information available on the last page of the article

Statement of Novelty

This manuscript reports an original experimental study obtained in the framework of the European project Waste-2Watts (Grant Agreement N° 826234), where the aim is to design and test a flexible and cost-effective cleaning unit to remove impurities for the use of biogas in high-efficiency fuel cell systems. The focus is on small to medium-sized farms for which deep biogas cleaning by adsorption materials is a suitable techno-economic solution to avoid intensive gas processing treatments. The work aims to verify whether a single sorbent reactor fed by humid gas (no chiller/drier installed within the plant) is suitable for that aim. Therefore, the authors explored in this work if a compromise exists between the "optimum operative conditions" of the sorbents (which leads to two vessels with an intermediate drier) and a simplified and low-cost solution (one single reactor) working with lower, but still suitable performance and a better economic assessment (lower CAPEX, slightly higher OPEX). Graphical abstract is attached as a file.

Introduction

Biogas production and use have increased rapidly in many countries over the last 20 years, enhancing its importance as a renewable energy source. The global installed biogas capacity reached 20.1 GW in 2020, 13.6 GW in Europe, 2.6 GW in North America, and 3.1 GW in Asia, Oceania, and Africa, as shown in the IRENA 2021 energy statistics [1]. According to the European Biogas Association 2021 Statistical Report, the total number of installed biogas plants in the EU is 19,654, with Germany leading with over 11,000 plants, followed by Italy and France (1710 and 861 plants, respectively) [2]. Kampman et al. [3] estimated a further doubling of biogas production in 2030, and even larger leaps could be possible in individual member states. The growth of the biogas market, especially in the EU, is favoured by both European and national support measures (RePowerEU, Fit-for-55 Package, Common Agricultural Policy, Renewable Energy Directive RED II) but also by inherent advantages that this technology brings, such as the recycling of waste into valuable products, which proves to be a smart example of a circular economy. It could also contribute to the production of green energy, biofuels, and heat.

A wide variety of organic materials can be used in anaerobic digesters as a feedstock for biogas production. More than 70% of EU biogas plants for electricity run on agricultural feedstock [4]. Integrating the biogas sector as part of sustainable agriculture can provide opportunities to reduce the greenhouse gas emissions from manure and waste and increase the use of biogas by-products for improved soil management (bio-fertilisers).

Today, most biogas is used for electricity and heat generation in cogeneration plants (more than 95% of the total number of plants according to European Biogas Association [2]) or upgraded to biomethane. This biofuel can be employed directly in the transport sector or injected into the natural gas grid to be used in the building sector (for heating/cooking purposes). Biomethane currently accounts for 17% of the total energy produced from biogas [5], and it is expected to increase, driven by several existing European and national incentives.

Despite a growing increase—driven by national incentives—of the biomethane plants at EU level, there are still some cases where biomethane production is not the cost-optimal solution, such as a high number of small- and medium- plants, usually running on agricultural biomass. In these cases, the locally available bioresources are responsible for a low biogas production ($<<100$ m^3/h and sometime <10 m^3/h) to justify the investment cost of a CH_4/CO_2 separation. In these circumstances, electricity generation seems to be the cost-optimal solution, especially if the energy produced can be self-consumed without depending on available incentives [6, 7]. Biogas is commonly exploited in Internal Combustion Engines (ICEs) for electricity production. The electrical efficiency of ICEs can exceed 40% for plants with an installed capacity of several hundred kW (>500 kW) and has a maximum of about 43% for MW installations, up to a few MW (<4 MW). Smaller combustion engines are indeed often economically disadvantageous because of their lower electrical efficiency (30–35%) [8]. In this context, fuel cells, especially Solid Oxide Fuel Cells (SOFCs) are an attractive alternative [9–12]. Since fuel cells are not limited by the thermodynamic Carnot efficiency, they have the highest electrical efficiency on the smallest scale (1 kW), compared to the currently widely used combustion technologies [13]. In addition, they have a high electrochemical capability to convert gas mixtures with fluctuating CH_4 heavily diluted with CO_2, and the heat generated by these devices can be used to heat the anaerobic digester, which could further increase the biogas yield, especially during the winter season. Last but not least, they can operate in reverse mode (producing H_2) in an integrated plant where a surplus of electricity is generated from others intermittent sources [14]. However, the main challenge in using biogas as fuel for SOFCs is that it contains various impurities that can lead to system degradation and failures. For biogas from agricultural waste and Organic Fraction of Municipal Waste (OFMSW), the main impurities are sulphur-containing compounds [8].

The most abundant sulphur compound is hydrogen sulphide (H_2S), which can reach thousands of ppm_v in the raw

gas from the digester. A few ppm_v of tricky non-H_2S traces such as CH_3–S–CH_3 (DMS dimethylsulphide), CH_3–SH (methyl mercaptan), COS (carbonyl sulphide) are also often present in the biogas [15, 16]. As far as H_2S removal is concerned, the choice of the purification techniques strongly depends on the H_2S load (input concentration) and the equipment in which the biogas is used (combustion engines, fuel cells, upgrading units or boilers). The removal of hydrogen sulphide has been studied in detail in the literature [17–19], by means of experimental and modelling activities [20–22].

In-situ abatement techniques are commonly used to partially remove H_2S directly in the anaerobic digester. Various techniques are used to achieve this goal. The most commonly used is the addition of iron salts directly into the digester, which can reduce the total S-content to about 100 ppm_v [23]. The in-situ abatement is often followed by a downstream purification section to reduce the concentration of impurities below the strict limits required for fuel cells (< 1 ppm_v) or for upgrading units [24].

The removal of sulphur species from biogas is more effective when a chemical reaction occurs directly on the surface of the adsorbent (catalytic reaction). The iron sponge process is an example of a chemical reaction on the surface of the adsorbent surface. It usually employs iron oxide (Fe_2O_3) or hydroxide ($Fe(OH)_3$) media, coated onto a supporting material traditionally comprised of clay, wood chips or wood shavings. As the biogas flows through the iron sponge, the hydrated iron oxide reacts with H_2S to form iron sulphide (FeS), thus removing H_2S from the gas [25]. Impregnated Activated Carbons (IAC) are examples of catalytic processes for efficient removal of H_2S from biogas. IACs are also commonly used to remove organic sulphur compounds such as CH_4S, C_2H_6S, CS_2, and COS, although lower removal efficiencies have been reported in the literature [24]. Activated carbons (ACs) are not selective by themselves, but their selectivity to certain contaminants and adsorption capacities can be improved by impregnating the carbon with selected compounds (KOH, NaOH, or otherwise modified) [26]. From this point of view, the chemical and physical characterisation of the different impregnated sorbents can be very useful to improve their performance toward sulphur compounds. Organic sulphur compounds, such as carbonyl sulphide (COS), even when present in biogas at concentrations two or three orders of magnitude lower than H_2S (usually a few ppm_v) are capable of poisoning and deactivating fuel cell catalysts [8]. In addition, COS is a toxic volatile sulphur compound, listed as a hazardous air pollutant under the Clean Air Act and has the potential of exploding under various mixing ratios with air [27]. Anyway, there are few studies in the literature on the removal of COS from a biogas stream. It can be removed by a potassium carbonate solution or amine treatment [28]. COS can also be converted to H_2S by catalytic hydrogenation or hydrolysis before H_2S is removed [29]. Due to the low polarity of COS, it cannot be adsorbed by most molecular sieve materials [30]. For this reason, finding an effective COS removal solid sorbent working in biogas real conditions such as at room temperature and humid conditions, eventually with the co-presence of other different sulphur compounds is still an issue [24, 31].

The EU Waste2 Watts project, launched in January 2019, aims to develop and test a complete small- to medium-sized system for biogas-to-energy valorisation through SOFC [32]. The project aims to find widely applicable and cost-effective solutions for the purification of biogas for SOFC use, employing methods and sorbents selected and characterised by specialised partners. One case study analysed in the project is the conventional small-scale farm, where the optimal purification solution is an adsorption system filled with solid sorbents. The three laboratories involved in the activity—POLITO (Italy), PSI (Switzerland) and ENEA (Italy)—were asked to test several solid sorbents against a specific contaminant, to check whether the same material could be effective in removing several contaminants, and to design a cleaning system with the minimum required sorbents. The one-vessel solution with one or more adsorbent materials for the removal of all contaminants is a goal pursued by this project. Therefore, we investigated the performance of the adsorbent materials even under non-optimal conditions in terms of oxygen and humidity to identify a suitable solution. To validate the proposed cleaning solution for agro-biogas, a cleaning unit is deployed at a selected demo site with a 6 kWe SOFC system from SOLIDpower and the cleaning performances are monitored using on-site gas analytics.

Table 1 Selected COS and H_2S removal sorbents

Sorbent name	Manufacturer	Type	Contaminant
KS3	Calgon/Chemviron	Impregnated activated carbon	COS
RGM3	Norit Dolder	Impregnated activated carbon	COS, H_2S
Ultra DS-6	Desotec	Impregnated activated carbon	COS, H_2S
R2D	SulfaTrap	Functionalized zeolite, molecular sieve	COS
R7H	SulfaTrap	Functionalized alumina	COS, H_2S
R8C	SulfaTrap	Impregnated activated carbon	COS
Bio-Clean	Biocustom	Iron hydroxide	COS, H_2S

Table 2 Operating conditions for the screening tests

Parameter	Value
Temperature of the sorbent bed	30 °C
Gas Hourly Space Velocity (GHSV)	1500 h^{-1}
Sorbent bed height over diameter ratio (H/D)	≥ 3
Gas matrix	CH_4/CO_2 mixture
CH_4/CO_2	50/50%
Oxygen content	0.5–1%
Gas Relative Humidity (RH)	40–50%
Inlet COS concentration	30 ppm_v
Inlet H_2S concentration	500 ppm_v

Table 3 Sample mass for the different sorbents in H_2S and COS adsorption runs (H/D = 3)

Sorbent	Sorbent mass (g)	
	H_2S removal tests	COS removal tests
Bio-Clean	17.0	6.01
KS3		4.26
R7H	37.2	7.31
RGM3	14.2	3.34
R2D		5.92
R8C		4.90
Ultra DS-6	15.8	4.21

This paper reports the results of the POLITO and ENEA experimental campaign and focuses on the removal of H_2S and COS, two of the most challenging contaminants in agro-biogas; the sorbents were selected based on a screening phase reported in a previous work by the authors [16].

In this work, the selected sorbents were characterised using different techniques and their removal capacities were tested in an experimental campaign in which different operating conditions were analysed under a common Design of Experiments (DoE). The removal capacities were correlated with the morphological and chemical properties of the sorbent surface to explain the adsorption mechanism.

The analysis is structured as follows: the first chapter presents the overall methodology in terms of sorbents, experimental setup and procedure and characterisation techniques. The second section deals with the experimental results, which are first presented separately for H_2S and COS and later discussed together in the final discussion chapter.

Materials and Methods

Sorbent Samples

Table 1 shows the selected sorbents involved in the experimental campaign, with information on the manufacturer, the material typology and the pollutants for which they have been studied.

Among the sorbents, seven were tested for COS removal and six for H_2S removal as they were selected within the Waste2Watts (W2W) project as candidates. Some sorbents were suggested by the producers for the removal of a specific contaminant (for example R8C for COS removal or R7H for H_2S removal).

For COS removal tests, all the sorbents were manually ground and sieved to obtain a 250–350 µm powder, while for H_2S removal, the sorbents are tested in pellet-shaped, as delivered by the suppliers. The sorbent characteristics are reported in Table S.1 in the Supplementary Material.

Methodology and Testing Conditions

The sorbent capacity (C_{ADS}, expressed in grams of contaminant removed per gram of sorbent) at the threshold outgoing contaminant concentration is derived from the breakthrough curve data and it is calculated using the following equation, shared among partners.

$$C_{ADS} = \int_{t_0}^{t_{BT}} A \cdot \left(CC_{in} - CC_{out}\right) dt \quad (1)$$

$$A = \frac{Q_{tot} \cdot MW}{V_m \cdot m} \cdot 10^{-6} \quad (2)$$

where:

- t_0: time at which the contaminant flow starts to pass through the sorbent bed (min)
- t_{BT}: breakthrough time, when the outlet contaminant concentration is 1 ppm_v for COS and 5 ppm_v for H_2S (min)
- CC_{in}: inlet contaminant concentration (ppm_v)
- CC_{out}: outlet contaminant concentration (ppm_v)
- Q_{tot}: total gas flow rate (L/min)
- V_m: molar volume (24.414 L/mol)
- m: mass of sorbent material (g)
- MW: molecular weight (60.1 g/mol for COS, 34.1 g/mol for H_2S).

A small quantity of the exhausted sample was preserved for post-adsorption characterisation analysis. The operating conditions for the screening tests, listed in Table 2, were shared among the W2W partners to define a common set of experimental test conditions for the different contaminant

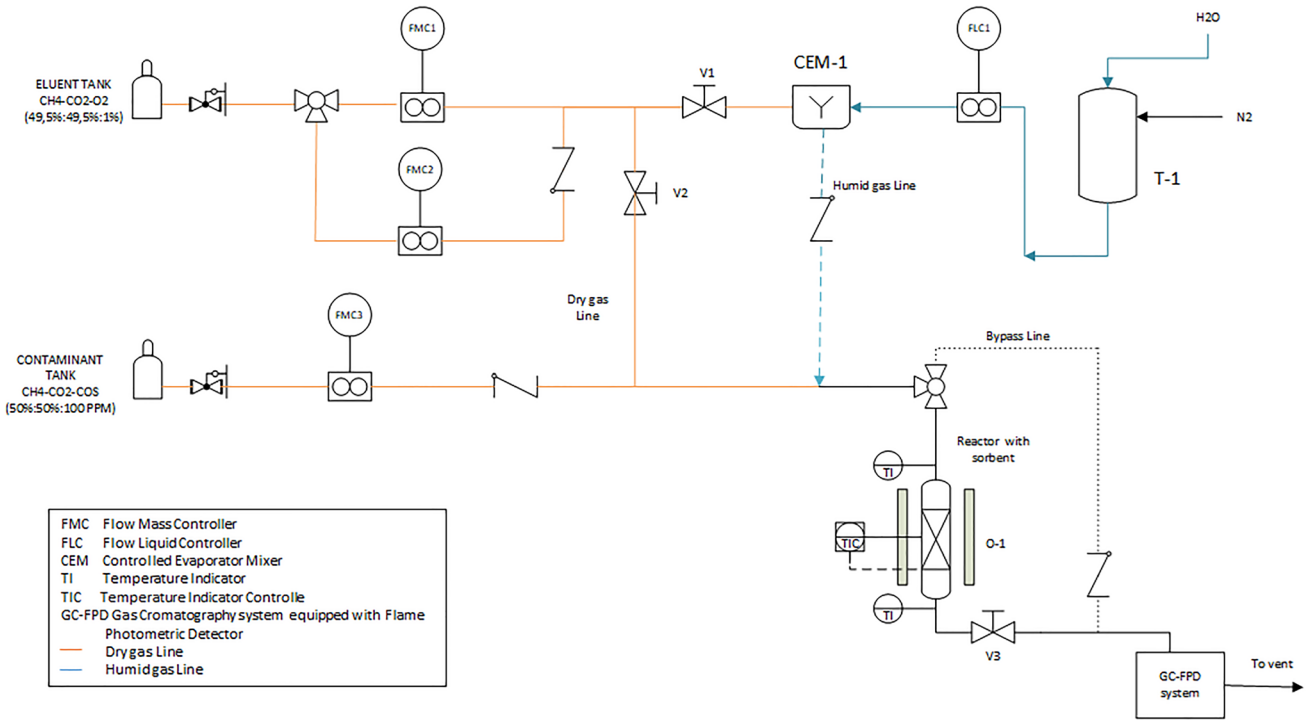


Fig. 1 Schematic diagram of the experimental test bench in ENEA

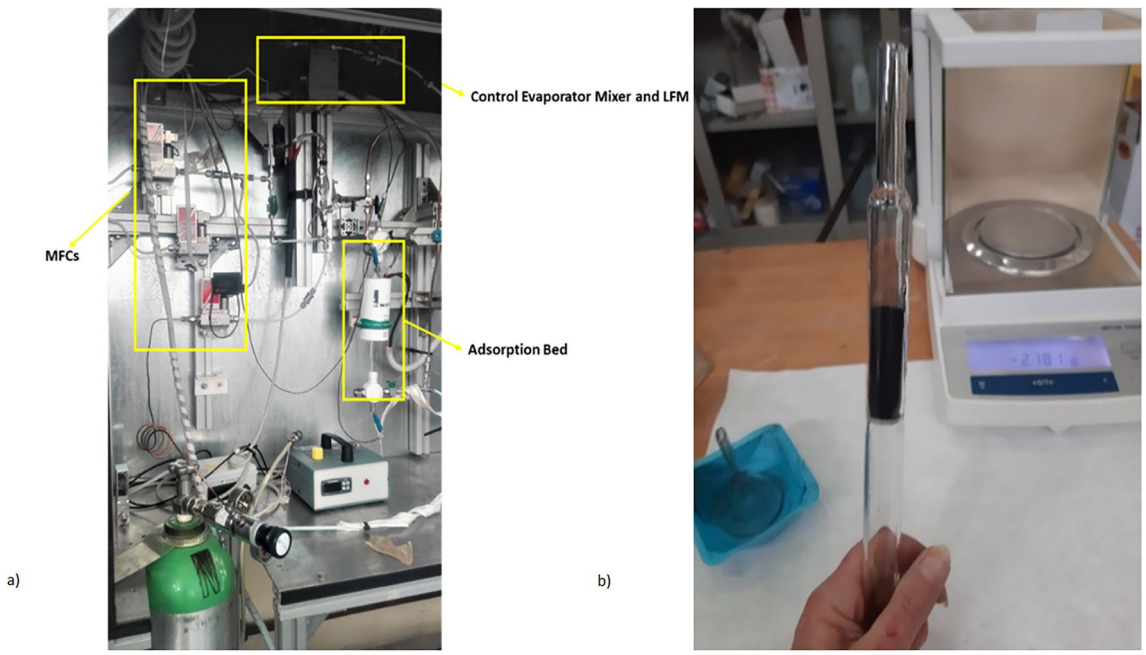


Fig. 2 Layout of the ENEA test unit: **a** Clean-up test bench, **b** Quartz reactor

uptake tests. The adsorption process is a complex phenomenon that depends on several parameters, including the initial concentration of the contaminant, the composition and humidity of the simulated biogas, the Gas Hourly Space Velocity (GHSV), the size of the reactor, the properties of the sorbent, and the breakthrough. The interplay of these factors makes it difficult to compare results between tests conducted under different conditions.

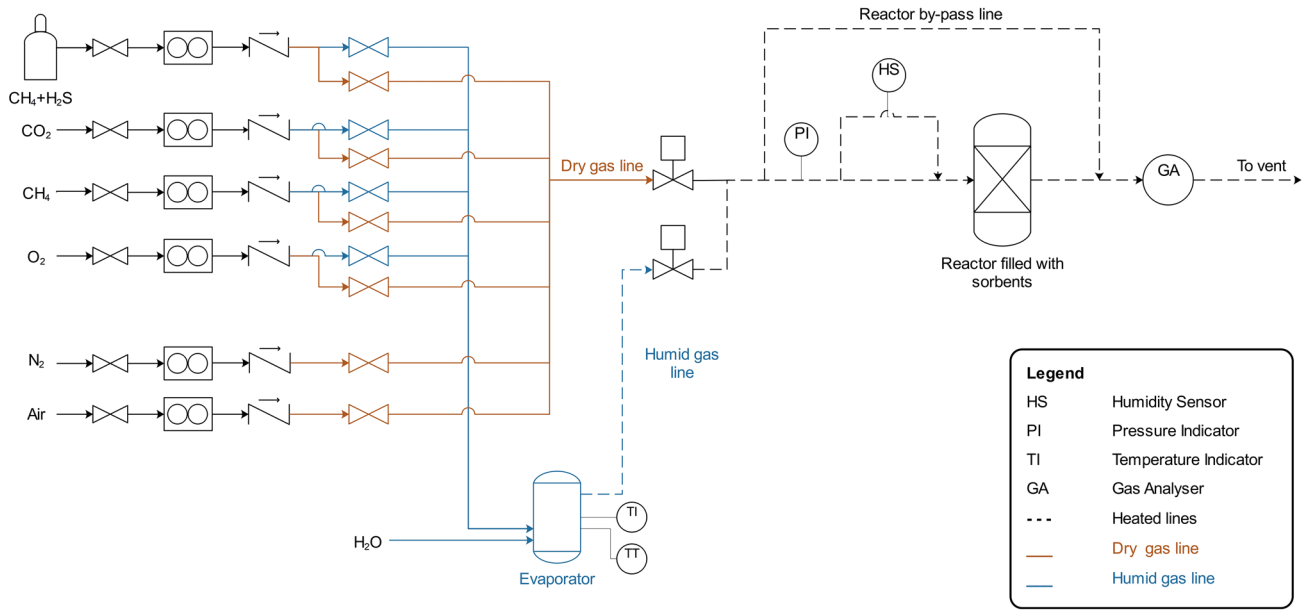


Fig. 3 Schematic diagram of the experimental test bench in POLITO

Table 3 lists the sorbent mass used in the H_2S (pellets) and COS (powder) adsorption tests for each sorbent.

COS Removal: Experimental Setup and Testing Procedure

A schematic flow diagram of the experimental setup for sulphur compounds removal tests at ENEA labs is shown in Fig. 1. The core of the system is a fixed bed quartz reactor (15 mm internal diameter and 100 mm length) with a quartz porous sieve (100–160 µm -G1 porosity) at half-length to place the powderbed. The external temperature of the reactor is controlled in the range 0–500 °C using a ceramic fibre heater (Watlow), and its internal temperature is measured through a thermocouple placed inside the reaction chamber. The temperature at the inlet and outlet of the reactor is monitored using two K-type thermocouples. The pollutant flow is supplied using a mixture of 100 ppm_v COS in CH_4–CO_2 (50:50) matrix and eluent (CH_4 49.5%–CO_2 49.5% + O_2 1%). To obtain the selected contaminant concentration the mixture is diluted with the eluent, using the three Mass Flow Controllers (MFCs) by Bronkhorst HIGH TECH. The amount of water needed to get the selected relative humidity conditions is provided using a liquid flow meter (LFM, Bronkhorst) and a Control Evaporator Mixer (CEM-Bronkhorst). Only the eluent stream passes through the CEM mixer; the gas containing sulphur contaminant is mixed after the CEM, before entering the reactor. Pipelines' temperature is controlled through Heating Tapes (HT) from the CEM to the reactor, to prevent water condensation inside the system. All the lines are made with Sulfinert® material to avoid adhesion of the contaminant on metal and to preserve the ppm_v level of sulphur compounds.

The output gas is analysed by the gas chromatograph (Perkin Elmer Clarus 680 GC) customised for continuous measurements of COS concentration; the instrument is equipped with a FPD detector (Flame Photometric Detector, specific for low-level sulphur detection).

The weighted mass of the 250–350 µm mesh sorbent powder was poured into the 15 mm diameter quartz reactor to cover the silicate filter placed at half-height of the reactor (Fig. 2b). The sorbent powder density was previously determined in order to set a sorbent mass suitable to have a 45 mm adsorbent bed height (H/D = 3). The reactor is then placed into the furnace and tightly connected to the inlet and outlet ¼" tubing. Any apparatus leakage is detected by flowing a 200 mL/min nitrogen flow both into the reactor and the by-pass circuit; the effect of the nitrogen flow is to purge the system and the reactor from residual contaminations.

H_2S Removal: Experimental Setup and Testing Procedure

The experimental setup of the test bench consists of a fixed-bed reactor with an inlet diameter of 22 mm and length of 115 mm, which is filled with the sorbent as received from the manufacturer (pellet shape). The schematic configuration is shown in Fig. 3.

The pollutant cylinder composition is 2000 ppm_v of H_2S in CH_4 matrix. This mixture is diluted with a simulated-biogas flow to obtain the inlet target concentration of the pollutant. The biogas flow is controlled by a set of mass flow

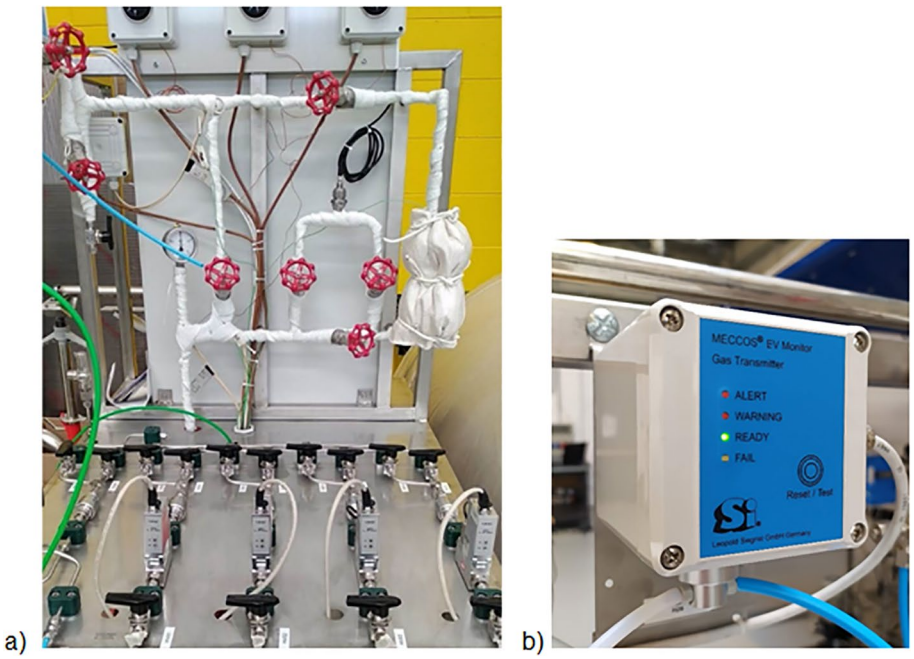


Fig. 4 **a** POLITO clean-up Test Bench. **b** MECCOS sensor H_2S detection from Siegrist GmbH

controllers (EL-FLOW—Bronkhorst) which supplies CO_2, CH_4, $CH_4 + H_2S$ and O_2 through dedicated lines.

The selected relative humidity in the gas flow is reached through a bubbler with an internal electric resistance heating for temperature control, able to saturate the incoming stream. Each line supplying the gas mixture is bifurcated into two sections: the wet line passes through the bubbler where the gas stream is saturated in water, and the dry line is joined directly to the reactor. The required humidity is reached by mixing the streams from the dry and the wet line by employing two solenoid valves. Only CH_4 and O_2 can be sent to the bubbler due to constraints related to the solubility of H_2S and CO_2 in water. The relative humidity is measured at the beginning of each test by a dedicated sensor (Vaisala), which is then bypassed during the test duration because of the risk of H_2S poisoning of the instrument.

The H_2S outlet concentration is measured by an H_2S sensor (MECCOS sensor from Siegrist GmbH) with a sensibility of 10% of full scale and able to detect H_2S concentrations ranging from 1 to 1000 ppm_v (Fig. 4).

The reactor and pipelines are held at 30 °C. The temperature of the lines is controlled through heating tapes to prevent water condensation inside the lines or in the H_2S sensor. The reactor temperature is controlled through a thermocouple, an insulated coating, and a dedicated heating tape. The bubbler temperature is maintained at 45 °C through electric resistance heating.

All the lines are internally coated by Sulfinert® material to avoid adhesion of the contaminant on metal and to preserve the level of sulphur compounds.

The reactor is filled with a weighted mass of the sorbent material pellets. The sorbent mass is set to obtain an adsorption bed length of 66 mm, to ensure a minimum H/D ratio of 3 to avoid preferential paths which limit the interaction between the sorbent and the gas stream.

The line setting and the gas mixture composition are managed according to the test conditions. The matrix gas mixture composition is 60% CH_4, 39.5% CO_2 and 0.5% O_2 in screening tests conditions. The amount of CH_4 has been increased at the expense of CO_2 to reach the target value of water in the biogas as only CH_4 stream can cross through the bubbler to be humidified. This solution should not significantly affect the sorbent performance as demonstrated by previous analysis [33]. With this gas composition, relative humidity of 40–45% is achieved. Although oxygen and steam are typically in the biogas and the H_2S removal process is expected to reach better performance in these conditions due to the involvement of chemisorption mechanisms, especially for activated carbons [31, 34, 35], the sorbent materials have been also tested in dry gas and absence of oxygen (50% CH_4 and 50% CO_2). This setting is expected to involve only physisorption processes and, therefore, the sorbent-bed saturation is expected to be faster.

The pollutant concentration is measured by the H_2S sensor and is recorded through the software FlexLogger. The adsorption capacity is obtained from the breakthrough curve data and is calculated according to Eq. (1) and Eq. (2). The breakthrough time is achieved when the contaminant concentration measured in the outgoing gas is 1% of the inlet H_2S concentration (5 ppm_v).

Table 4 Specific surface area and pore dimension of the selected sorbent materials

Sorbent	Specific surface area (m2/g)	Pore size (nm)
Ultra DS-6	786 ± 10%	3
RGM3	1006 ± 3%	3
Bio-Clean	130	8
R7H	30	8
R2D	370	–
KS3	736 ± 6%	3
R8C	689 ± 1%	3

Table 5 Main functionalizing element found on sorbent surface

Sorbent	Main element found on sorbent surface
Bio-clean	Ca
KS3	Fe
R7H	Cu
RGM3	Cu
R2D	Cu
R8C	K
Ultra DS-6	K

At the end of each test CO_2 and air are used to flush the pipelines and the H_2S sensor. A small quantity of the exhausted sorbent sample is preserved for post-adsorption characterisation analysis.

Characterisation Techniques

The sorbents have been characterised by N_2 adsorption/desorption, Scanning Electron Microscopy (SEM), Energy Dispersive Spectrometry (EDS) and Thermo Gravimetric Analysis (TGA) to get information about their specific surface area and bulk and surface composition. Characterisation analyses were performed both in POLITO and ENEA, following the same techniques described in the section below.

Surface area and pore size distributions were analysed with Micromeritics Tristar II 3020 instrument (in ENEA) and with ASAP2020 Plus Micromeritics analyser (in POLITO). The Brunauer-Emmet-Teller (BET) and Barrel-Joyner-Halenda (BJH) methods were utilised to obtain specific surface area and pore size distribution, respectively, from N_2 physisorption isotherms. The analyses were conducted under liquid nitrogen temperature (77 K) with nitrogen as adsorbent gas. The sample was first degassed for about 2 h under vacuum at a temperature of 110 °C (ENEA) or for 3 h under vacuum at 200 °C (POLITO).

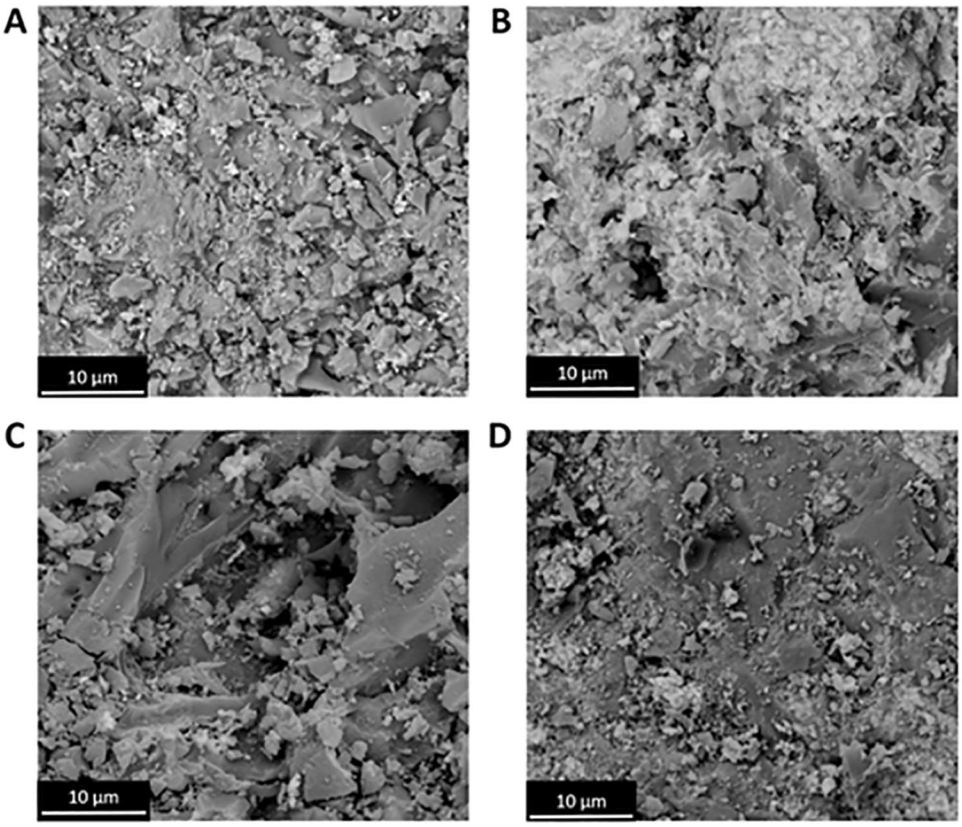


Fig. 5 SEM images with a magnification of 5000X: **A** RGM3 **B** RGM3_H_2S, **C** RGM3_H_2S_O_2 and **D** RGM3_H_2S_O_2_H_2O

Table 6 Average of three measurements of the atomic % revealed by EDS

Element	Atomic % (NORIT)	Atomic % (NORIT_H_2S)	Atomic % (NORIT_H_2S_O_2)	Atomic % (NORIT_H_2S_O_2_H_2O)
C	43	42	34	36
O	28	22	32	20
Cu	16	18	9	9
Si	2	1	1	2
K	3	2	1	1
Ca	2	1	1	3
P	0.4	0.5	0.3	1
S	3	14	23	29

The SEM analysis was performed using a Tescan Vega 3 (ENEA) and a PhenomXL (POLITO) with lanthanum hexaboride (La_6B) source. For additional information see Section S.2 in the Supplementary Material.

The TGA was performed using a Pyris 1 instrument from Perkin-Elmer (Waltham, Massachusetts). Briefly, thermal analyses were performed by heating from 30 to 800 °C (rate: 20 °C/min) approximately 10 mg of samples under nitrogen flux (35 mL/min). The gases released during the heating ramp was piped (gas flow: 65 ml/min) via pressurised heated transfer line (Redshift S.r.l., Vicenza, Italy) and analysed continuously by the FTIR (Fourier-Transform Infrared) spectrophotometer (Spectrum 100; Perkin-Elmer). FTIR spectra were acquired in the range of 4000–600 cm^{-1} and analysed with the instrument software (Perkin-Elmer). CO_2 gas was excluded by the IR (Infrared) detector to avoid the associated signal noise not allowing the proper detection of other released gases.

Results

Sorbent Characterisation Results

Material functionalisation and specific surface area affect the uptake capacity of sorbent materials. Therefore, SEM–EDS and N_2 adsorption–desorption analyses have been conducted on the sorbents. The results obtained in terms of specific surface area (calculated by BET model) and average pore dimension are listed in Table 4.

The results of SEM–EDS analysis, presented in Section S.2 in the Supplementary Material, allowed to individuate the elements the functionalizing compounds consist of, even though the chemical composition of the compounds could not be inferred from this analysis technique. Effective functionalising compounds are known only for RGM3, R2D and R7H, as they can be found on sorbent data sheets, unknown for the remaining sorbent. Table 5 reports the main element found on sorbent surface, after eliminating the main scaffold element (i.e., carbon for AC).

Table 7 Specific surface area, pore volume, and pore size of the RGM3 samples tested in different conditions

Sample	Specific surface area (m^2/g)	Pore volume (cm^3/g)	Pore size (nm)
RGM3	940	0.455	3.0
RGM3_H_2S	855	0.452	2.8
RGM3_H_2S_O_2	720	0.385	2.9
RGM3_H_2S_O_2_H_2O	469	0.233	3.0

Post-Adsorption RGM3 Characterisation

In order to evaluate the ability of the sample to adsorb the H_2S molecule, RGM3 was tested in different conditions obtaining three samples: RGM3 placed in contact with the H_2S molecule without (RGM3_H_2S) or with (RGM3_H_2S_O_2) oxygen molecules and with oxygen molecules in an environment with 40% of humidity (RGM3_H_2S_O_2_H2O).

The samples after H_2S adsorption and the sample (RGM3) before adsorption (as blank reference sample) were characterised by SEM–EDS analysis (Phenom XL), N_2 adsorption/desorption analysis, and TGA coupled with IR spectrometer.

SEM images of pellet or fragmented samples showed a not homogeneous surface similarity between the blank and the samples after adsorption, without relevant differences (Fig. 5).

A relevant difference was evidenced by EDS analysis of the investigated samples (Table 6), which reveal for RGM3_H_2S, RGM3_H_2S_O_2, and RGM3_H_2S_O_2_H_2O a significantly higher amount of S compared with RGM3, as

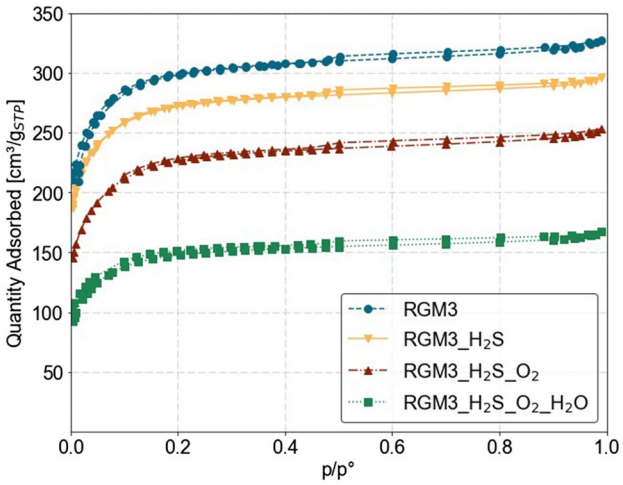


Fig. 6 Isotherms of RGM3 before (blank sample) and after testing

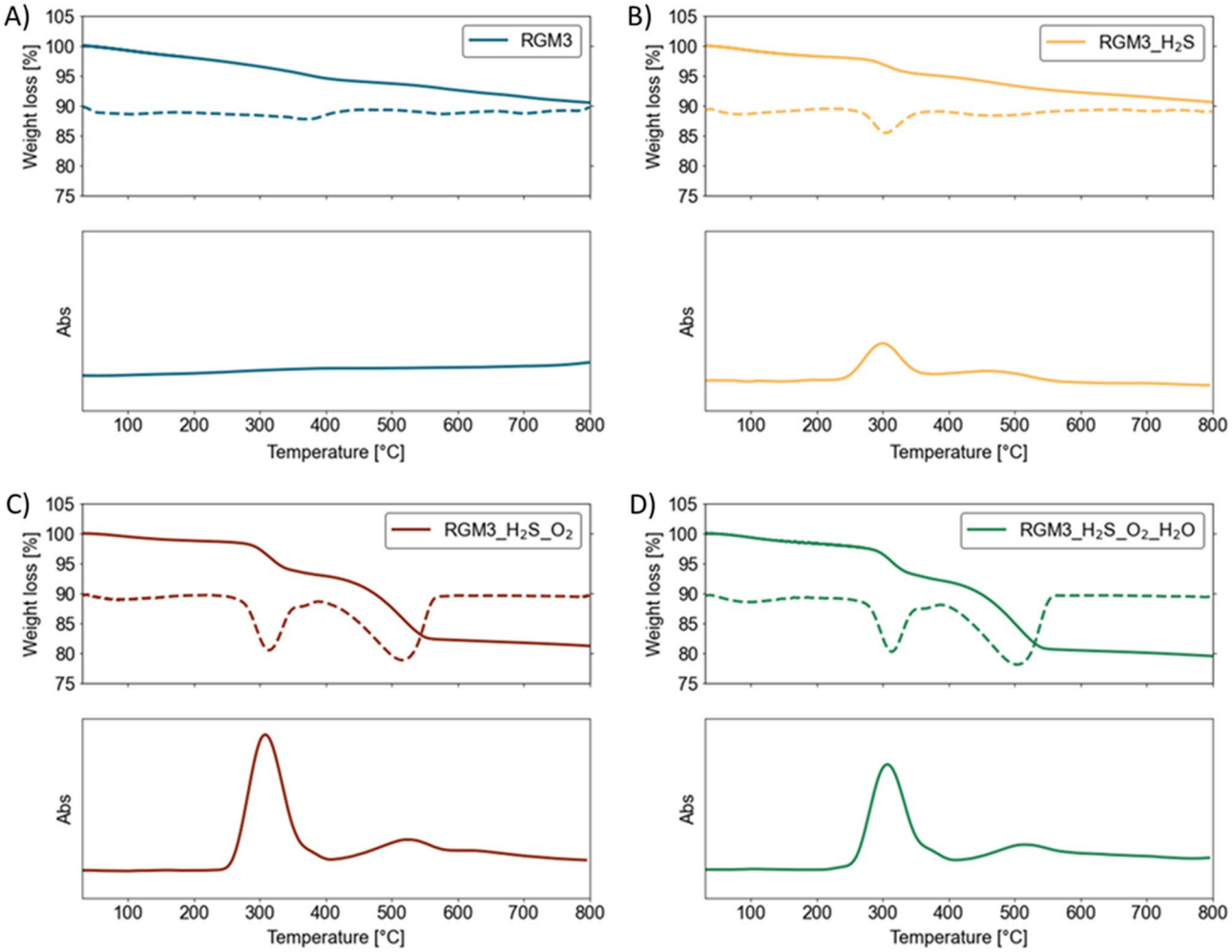


Fig. 7 **A**–**D** graphs above are related to TGA (solid line) and DTGA (dashed lines) of the different samples. On the x-axis is reported the temperature and on the y-axis is reported the % of weight loss. **A**–**D** graphs below: temperature/time-resolved absorption IR band at 1376 cm^{-1} in the temperature range. On the X-axis is reported the temperature and on the Y-axis is reported the absorbance

a consequence of H_2S adsorption. Furthermore, the atomic percentage of elemental sulphur of RGM3_H_2S_O_2 and RGM3_H_2S_O_2_H_2O is significantly higher compared to RGM3_H_2S. These data suggest a greater absorption of H_2S in presence of O_2.

N_2 adsorption/desorption analysis isotherms revealed, as expected, a decrease in the specific surface area for the samples placed in contact with H_2S compared to the blank sample (Fig. 6).

The results indicate a progressive decrease of the specific surface area and pore volume of the samples tested in the presence of oxygen and humidity, as compared to RGM3 and RGM3_H_2S, suggesting a greater absorption of H_2S gas when in contact with oxygen molecules (Table 7). The adsorption process does not significantly affect the pore size distribution, as only a fraction of pores is blocked by the molecule adsorption, while the remaining fraction remains basically uneffaced. Therefore, the shape and size of the pores unaffected by blockage remain essentially unaltered.

A TGA was performed to evaluate the capacity of the sample to adsorb the H_2S molecule in different conditions and IR analysis was performed on the gas released during the thermal treatment. The TGA analyses and related derivative curves show some significant differences for the investigated samples (as shown in Fig. 7—graphs above). In fact, RGM3_H_2S_O_2 and RGM3_H_2S_O_2_H_2O showed a larger weight loss (3.2% for both samples) in the 270–360 °C range compared with RGM3_H_2S (0.9%). In addition, the first derivatives show that at variance with RGM3_H_2S, the adsorbents tested in the presence of oxygen show negative peaks (the first at around 300 °C and the second at around 500 °C), with those centred at higher temperatures associated with larger weight losses. In particular, the samples also contacted with oxygen evidence in the temperature range

400–550 °C a weight loss of 8.9% (RGM3_H_2S_O_2) and 9.9% (RGM3_H_2S_O_2_H_2O) compared with RGM3_H_2S (0.8%). The gases emitted during the TGA were then analysed continuously by the FTIR. Data were then plotted in temperature/time-resolved spectra.

The temperature/time-resolved spectra of the gases released during the overall analysed temperature range showed that the samples contacted with H_2S, namely RGM3_H_2S, RGM3_H_2S_O_2, and RGM3_H_2S_O_2_H_2O release sulphur dioxide gas (SO_2) at variance with RGM3. The presence of SO_2 during the release is due to the adsorption of H_2S gas on the samples surface and its dissociation during the dissolution in the water layer adsorbed into the pores. Then an oxidation reaction occurs due to the adsorbed oxygen or metals present at the surface of the activated carbon, i.e. Cu which can acts as an oxygen-donor, in order to form elemental sulphur or sulphur dioxide [36]:

$$H_2S_{(g)} \rightarrow H_2S_{(ads)} \tag{3}$$

$$H_2S_{(ads)} \rightarrow H_2S_{(ads-liq)} \tag{4}$$

$$H_2S_{(ads-liq)} \rightarrow HS^-_{(ads)} + H^+ \tag{5}$$

$$HS^-_{(ads)} + O^*_{(ads)} \rightarrow S_{(ads)} + OH^- \tag{6}$$

$$HS^-_{(ads)} + 3O^*_{(ads)} \rightarrow SO_{2(ads)} + OH^- \tag{7}$$

where $H_2S_{(g)}$ is H_2S in gas form, $H_2S_{(ads)}$ is H_2S adsorbed on the activated carbon surface, $H_2S_{(ads-liq)}$ is H_2S dissolved in the water film, $HS^-_{(ads)}$ is the dissociated H_2S adsorbed, $O^*_{(ads)}$ is dissociatively adsorbed oxygen, $S_{(ads)}$ is the elemental sulphur adsorbed and $SO_{2(ads)}$ is sulphur dioxide adsorbed. The TGA analysis indicates that the moisture content significantly improves the adsorption capacity of the RGM3 sorbent, which could be explained by the requirement of a water film on the adsorbent surface for mechanism steps (4) and (5) to occur.

A preliminary IR analysis of the released gas species in the range 4000–600 cm^{-1} revealed only the band associated with sulphur dioxide. Then for each sample, an IR temperature/time-resolved spectrum was registered to analyse over time the peak detected at 1376 cm^{-1} (as shown in Figure Y-graphs below). Related spectra revealed an intense absorption due to released SO_2 at around 300 °C, followed by a signal of lower intensity in the 400–550 °C range. However, the second low-intensity signal does not correlate with the large weight loss observed in the 400–550 °C range, suggesting the release of an additional gas besides SO_2. CO_2 was initially excluded by the IR detector to avoid excessive instrumental noise. However, it is reasonable to assume that

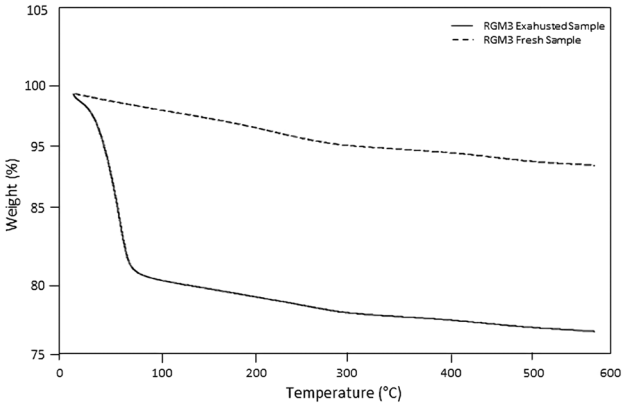


Fig. 8 Thermogravimetric analysis (TGA) of the RGM3 pre and post COS-adsorption test

the observed weight loss is ascribable to the release of CO_2 gas (although not detected by IR). The fact that the CO_2 adsorption is not visible in the RGM3_H_2S compared with RGM3_H_2S_O_2 and RGM3_H_2S_O_2_H_2O can be clarified considering the solubility of H_2S in the adsorbed water layer, which is higher than CO_2 solubility [37], leading to the adsorption of only H_2S for RGM3_H_2S.

In order to investigate the COS adsorption nature, if chemisorption or physisorption, the AC samples were analysed using the TGA before and after the COS adsorption process. Before each analysis, the carbons (both the pre and post COS adsorption) were left in a dry chamber at room temperature, to reduce their water content. The TGA curves of the post-COS adsorption samples are comparable with the blank ones. In fact, the exhausted carbon weight-loss runs

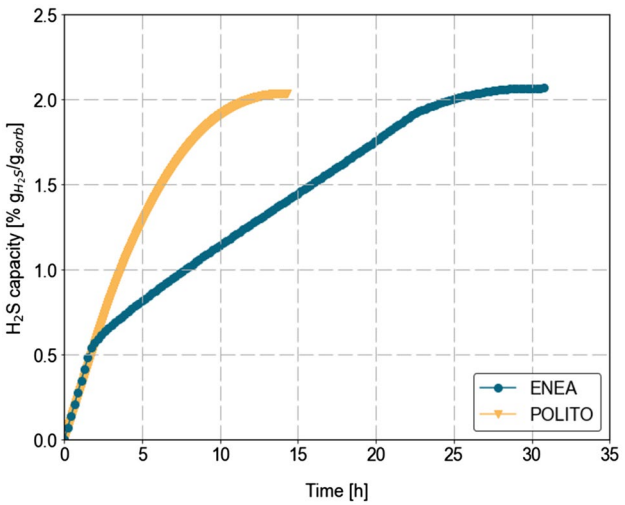


Fig. 9 Baseline test results. Tests were performed with Norit RST sorbent in the following operating conditions: H/D = 3; GHSV = 1500 h^{-1}; Contaminant = H_2S, 500 ppm_v (see Section S3 in the Supplementary Material)

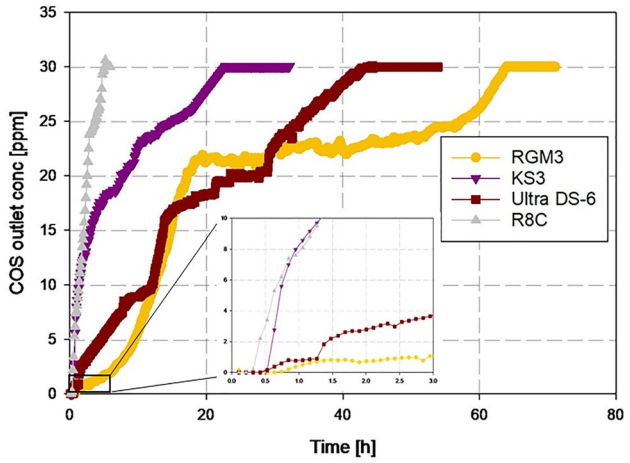


Fig. 10 ACs Breakthrough curves of the four ACs in the screening tests conditions

out within 100 °C and it is consequently ascribable or not distinguishable from pure water desorption. In Fig. 8 curves obtained from the fresh and COS-exhausted RGM3 sorbent are shown as an example of the results obtained from TGA analysis.

The COS deposited on the surface is desorbed both during the pre-heating, by flushing the sample with an argon stream, and by the first desorption step within 100 °C, indistinguishable from the water release; no evidence of COS dissociation and S reaction over the sorbent surface (chemisorption) was detected.

Adsorption Test Results

A first baseline test comparison was performed among the two laboratories, to verify the reliability of the experimental campaign. ENEA tested powdered sorbents in a microreactor, while POLITO tested pellet sorbents (as received from the suppliers) in a small-scale reactor. The goal was to compare the breakthrough and saturation adsorption capacities results obtained on the same sample with the same nominal conditions with the two labs experimental facilities. Results from the baseline tests are shown in Fig. 9. The error between the adsorption capacities values is around 5% at the breakthrough time and lower than 2% at saturation.

Screening Tests Results

The first part of the experimental campaign was the screening of the sorbent materials selected on their COS and H_2S uptaking capacity, using the reference conditions described in Table 2.

COS Removal The zeolite (R2D), alumina (R7H), and iron-based (Bio-clean) sorbents turned out to be totally transparent to COS, showing no sorption capacity at all. Being utterly inadequate as adsorbents with respect to COS the results of the tests on those sorbents are not reported in this work. Activated carbon sorbents removed COS totally until breakthrough, as reported in Fig. 10.

The difference between the two sets of sorbents is attributed more to the morphological nature of the sample than to its composition: the ACs exhibit a high porosity and their specific area surfaces are more than twice the zeolite/alumina/iron hydroxide sample one, as the BET results in Table indicate. As reported there, the four ACs samples present similar specific surface areas, slightly larger for RGM3 and Ultra DS-6 and lower for KS3 and R8C, the same trend of the capacity results.

Table 8 reports the tested sorbents' breakthrough time and adsorption capacity. The main error affecting the measured values is the ± 6 min in the measuring time scan. This factor obviously affects mostly the low time values, as the worst performance at 1 ppm_v breakthrough, respect to the high time values obtained at carbon saturation.

The calculated capacities at 1 ppm_v outgoing contaminant concentration of the four ACs range from 0.83 mg of COS per sorbent gram of the best sample, the RGM3, to 0.16 mg of COS per sorbent gram of the worst sample, the KS3.

In terms of sulphur removal this means that about 0.4 mg of sulphur for each sorbent gram is hindered to pass through the RGM3 bed. These capacity values result much lower than those measured on the same AC against H_2S, suggesting that no chemical reaction but only weak intermolecular

Table 8 ACs breakthrough times, at 1-ppm_v outgoing contaminant concentration and when the outgoing contaminant concentration reached the incoming level, COS adsorption capacities calculated at the same points (Test conditions: GHSV 1500 h^{-1}; COS C_{in} = 30 ppm_v, T = 30 °C, RH = 50%)

Sorbent	$t_{bt\ 1\ ppm}$ (h)	$t_{bt\ 100\%}$ (h)	$C_{ads\ 1\ ppm}$ (g_{COS}/g_{sorb}) %	$C_{ads\ 100\%}$ (g_{COS}/g_{sorb}) %	$C_{ads\ 1\ ppm}$ (g_S/g_{sorb}) %
RGM3	2.95	64.04	0.083 ± 3	0.69	0.044 ± 0.15
Ultra DS-6	1.37	43.57	0.031 ± 7	0.41	0.016 ± 0.22
KS3	0.63	22.68	0.016 ± 15	0.16	0.008 ± 0.44
R8C	1.2	14.7	0.023 ± 10	0.11	0.012 ± 0.68

Table 9 Breakthrough time and H_2S adsorption capacity at 5 ppm_v (1% of inlet concentration) outgoing contaminant concentration at screening tests conditions

Sorbent	$t_{bt\ 1\%}$ (h)	$C_{ads\ 1\%}$ (g_{H2S}/g_{sorb}) %
Ultra DS-6	47.90	8.42
Bio-clean	66.7*	10.9*
RMG3	90.52 ± 4.16	17.71 ± 0.82
R7H	30.58 ± 5.43	2.35 ± 0.34

*BT defined as the time when the outlet contaminant concentration is 5 ppm_v after the initial peak

Van der Waals forces are involved in the COS adsorption process.

Figure 10 shows the breakthrough curves for the ACs tested; the curve onset is zoomed to show the 1 ppm_v outgoing contaminant concentration area. The breakthrough time at 1 ppm_v is not significantly different among the four samples; a much more pronounced difference arises from their saturation capacity values and from the shape of the curves.

The shape of the breakthrough curve could reveal something on the physisorption process and its time development The curves exhibit a more or less long plateau, depending on the analysed sorbent: RGM3 shows a flat plateau from 1000 to about 3500 min; Ultra DS-6 curve shows three plateaus, less flat and much shorter in time; the KS3 and R8C curves exhibit different slopes in approaching the saturation, rather than a plateau.

The plateau occurring at a definite outgoing contaminant concentration, could be ascribed to a COS-COS molecules interaction. The adsorption process is supposed to be split into four phases: in the first phase the whole contaminant in the incoming gas is retained by the sorbent surface, producing a zero COS concentration in the outgoing gas; when

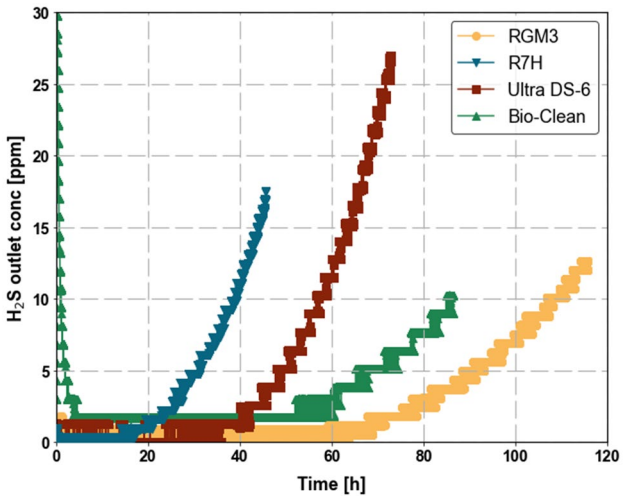


Fig. 11 Average breakthrough curves at screening tests conditions

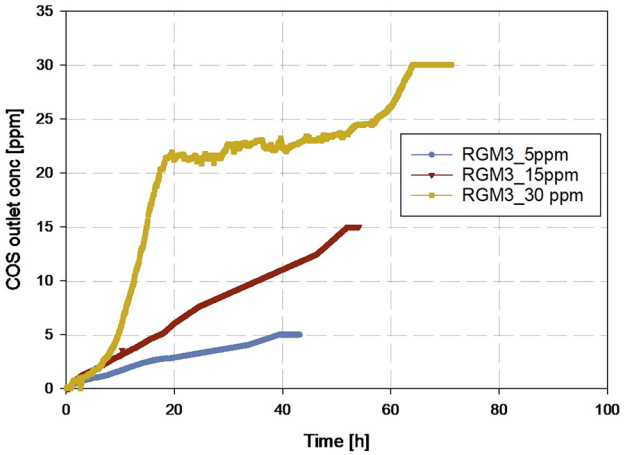


Fig. 12 RGM3 Breakthrough curves obtained using different COS concentrations (GHSV: 1500 h^{-1}; T: 30 °C, CH_4/CO_2:50/50 RH: 50%)

the active area is saturated the newly incoming COS molecules are retained in some percentage by the first layer of the adsorbed COS molecules; a rapid increase is detected till this percentage is reached. Then for a while, the plateau time, this second COS molecules layer covers the sorbent surface. When also these adsorption sites are saturated the outgoing contaminant concentration rises to the incoming level [38].

H_2S Removal Figure 11 shows the average breakthrough curves of the tested sorbents under oxygen and humidity conditions. Tests were interrupted before reaching saturation due to operational difficulties in carrying out tests of longer duration.

Among the tested sorbents, the Cu-functionalized RGM3 activated carbon exhibited the best performance, with an average adsorption capacity of 177.1 $mg_{H2S}/g_{sorb,}$ which is nearly double that of the K-functionalized Ultra DS-6 sorbent.

On the other hand, the copper-based sorbent R7H demonstrated poor performance under these conditions, with an adsorption capacity 7.5 times lower than RGM3. However, the R7H breakthrough time is only 3 times lower than RGM3, as the high packing density of R7H pellets allows for a higher amount of sorbent to be inserted into the same reactor volume.

The iron hydroxide Bio-clean sorbent is transparent to H_2S in the first 8 min of the tests. After the initial peak, the H_2S outlet concentration decreases to 1.7 ppm_v (plateau) before starting the exponential growth. In the first phase, the sorbent temperature increases due to chemical reactions, when the material is activated, the H_2S uptake occurs. This trend has been verified in different test repetitions and a similar trend is reported for O_2 adsorption in [39]

Table 10 COS concentration variation used RGM3 breakthrough times, at 1-ppm$_v$ outgoing contaminant concentration and when the outgoing contaminant concentration reached the incoming level and COS adsorption capacity

Sorbent	COS C_{Inlet} (ppm_v)	$t_{bt\ 1\ ppm}$ (h)	$t_{bt\ 100\%}$ (h)	$C_{ads\ 1\ ppm}$ (g_{COS}/g_{sorb}) %	$C_{ads\ 100\%}$ (g_{COS}/g_{sorb}) %
RGM3	30	2.95	64.04	0.083 ± 3	0.69 ± 0.15
RGM3	15	2.21	53	0.031 ± 4.5	0.4 ± 0.18
RGM3	5	4.5	39.3	0.02 ± 22	0.08 ± 0.25

(Test condition: GHSV 1500 h-1; T = 30 °C, CH_4:CO_2 50:50)

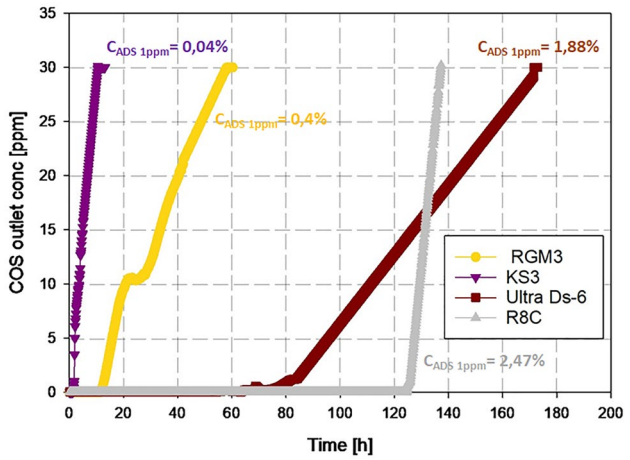


Fig. 13 ACs Breakthrough curves of the four ACs in the screening tests conditions without water (RH = 0%)

and a more in-depth analysis of the material characteristics should be performed to provide information on the adsorption mechanism. However, as the Bio-Clean performance is moderate and it is transparent to COS, no further information is reported.

Table 9 reports the breakthrough time and the adsorption capacity of the tested sorbents under screening conditions.

Sensitivity Analysis on Inlet Gas Composition

Variable Inlet COS Concentration The sorbent chosen for this experimental campaign was RGM3 as it is the one that showed the best performance in COS uptaking during the screening tests in a RH = 50% gas stream. The COS concentration was lowered to 15 ppm_v and 5 ppm_v, keeping all the other testing conditions unchanged. The breakthrough curves for the three different COS concentration tests are shown in Fig. 12, while Table 10 reports the COS adsorption capacity results.

The effect of inlet COS concentration on the dynamic adsorption process is significant; in fact, the calculated C_{ads} decrease by reducing the COS partial pressure in the gas stream.

COS Removal in Dry Conditions With the aim of understanding the role of water on the COS uptaking, the ACs were tested in dry conditions, keeping all the other testing parameters unchanged. The breakthrough curves and the relative C_{ADS} are shown in Fig. 13.

Comparing the C_{ADS} obtained at 1 ppm_v values, in dry conditions with those obtained in humid ones is evident that the performances improve a lot in absence of water for all the tested carbons, demonstrating competition between water and COS for the ACs physisorption sites. In particular, the C_{ADS} increment is about 3 times higher for KS3 and 5 times higher for RGM3. Ultra DS-6 and R8C sorption capacities are significantly higher in dry gas (about 60 and 100 times higher, respectively) than in humid gas. This result could be explained on the base of the sorbent functionalizing oxides. It's evident how the K functionalized ACs, namely Ultra DS-6 and R8C are largely more effective in COS uptaking than the Cu functionalized AC, but only in dry conditions. To investigate the adsorption phenomena occurring during the tests, the exhausted samples were subjected to desorption tests with the aim of tracking the sulphur compounds at the outlet of the desorption system. These tests were carried out with the adsorption tests apparatus just after the adsorbing

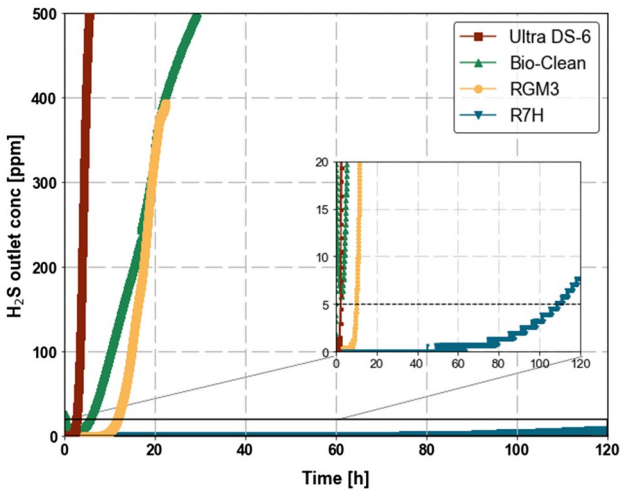


Fig. 14 Average breakthrough curves of the sorbents tested for H_2S removal under screening test conditions without water and oxygen

Table 11 Breakthrough time and H_2S adsorption capacity at 5 ppm_v outgoing contaminant concentration and when the outgoing contaminant concentration reached the incoming level (500 ppm_v)

Sorbent	$t_{bt\ 1\%}$ (h)	$t_{bt\ 100\%}$ (h)	$C_{ads\ 1\%}$ (g_{H2S}/g_{sorb}) %	$C_{ads\ 100\%}$ (g_{H2S}/g_{sorb}) %
Ultra DS-6	2.35	5.52	0.41	0.73
Bio-clean	0	29.15	0	2.71
RGM3	12.21 ± 2.71	25.65 ± 3.24	2.57 ± 0.22	4.11 ± 0.06
R7H	104 ± 13.16	N/A	7.77 ± 0.99	N/A

Test condition: GHSV 1500 h^{-1}; CH_4:CO_2 50:50; RH = 0%; O_2 = 0%; H_2S C_{in} = 500 ppm_v; T = 30 °C

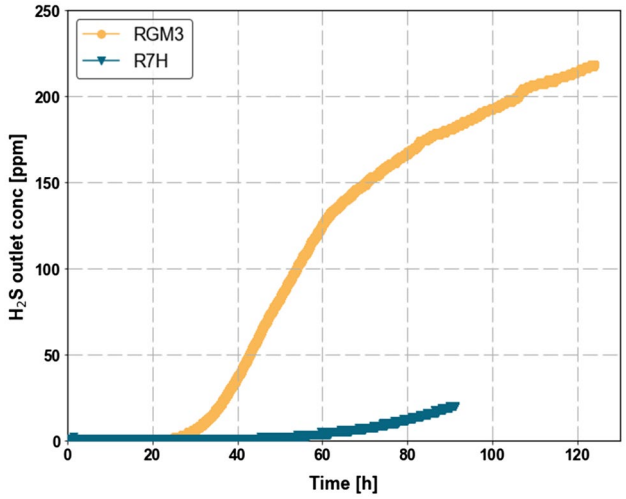


Fig. 15 Average breakthrough curves of the sorbents tested for H_2S removal under screening test conditions without water

tests. The AC spent samples were kept in the quartz reactor, and the AC bed was heated with increasing temperature steps at 50 °C, 100 °C, 150 °C and 200 °C, leaving it in temperature for 15 min for each step in a nitrogen flow. The outgoing flow was detected with GC-FPD detector to check sulphur compounds eventually formed during the adsorption process over the AC surface. Except for COS, no other sulphur compound was detected during the test.

Table 12 Breakthrough time and H_2S adsorption capacity at 5 ppm_v outgoing contaminant concentration test condition: GHSV 1500 h^{-1}; CH_4:CO_2 50:49.5; RH = 0%; O_2 = 0.5%; H_2S C_{in} = 500 ppm_v; T = 30 °C

Sorbent	$t_{bt\ 1\%}$ (h)	$C_{ads\ 1\%}$ (g_{H2S}/g_{sorb}) %
RGM3	28.33	5.55
R7H	59.69	4.45

H_2S Removal in Dry and Anaerobic Conditions Figure 14 shows the average breakthrough curves of the tested sorbents in dry and anhydrous conditions; the curve onset is zoomed to show the 5-ppm_v outgoing contaminant concentration section.

The R7H sorbent demonstrated good performance under these conditions, with an adsorption capacity of 77.7 mg_{H2S}/g_{sorb}, which is almost three times the H_2S uptake capacity of the RGM3 activated carbon. Therefore, despite the manufacturer's private information indicating that the adsorption capacity of the R7H sorbent would not be affected by oxygen or humidity, the test results revealed a negative impact of these factors on its performance.

The iron hydroxide Bio-Clean sorbent shows a similar trend as the screening conditions: it is transparent to H_2S in the first 5 min of the tests. After the initial peak, the H_2S outlet concentration decreases to 5 ppm_v (plateau) before starting the exponential growth. Breakthrough time and the adsorption capacity of the tested sorbents are summarized in Table 11.

Table 13 Summary of breakthrough (BT) and saturation (SAT) adsorption capacities ($g_{contamintant}/g_{sorb}$ %) for the different sorbents tested, under both dry and wet conditions

	COS			H_2S		
	Dry	Wet		Dry		Wet
	$C_{ads,BT}$	$C_{ads,BT}$	$C_{ads,SAT}$	$C_{ads,BT}$	$C_{ads,SAT}$	$C_{ads,BT}$
RGM3	0.40	0.083	0.69	2.57	4.11	17.71
Ultra DS-6	1.88	0.031	0.41	0.41	0.73	8.42
KS3	0.040	0.016	0.16			
R8C	2.47	0.023	0.11			
Bio-Clean				0	2.71	10.9
R7H				7.77		2.35

The white areas represent combinations that have not been explored as discussed in the previous chapters

Both RGM3 and R7H sorbents were tested under dry and aerobic conditions (50% CH_4, 49.5% CO_2 and 0.5% O_2). Indeed, as shown in Table 12, RGM3 showed good performance under screening test conditions and is a suitable sorbent for COS removal, while R7H exhibited the best performance for H_2S uptake in dry and anaerobic test conditions. Although both materials are functionalized with oxygen-donor metals, which suggests that their performance would be similar under anaerobic conditions, we were interested in investigating this condition due to the potential cost of insulating the system from air, that is higher than the cost of dehumidifying the stream. If good performance can be achieved under oxygen conditions, it could represent a viable solution (Fig. 15).

The RGM3 performance is enhanced both by oxygen and humidity. The performance under aerobic condition is 3 times lower than the screening test but exhibit a double adsorption capacity compared to the dry and anaerobic test conditions. The enhancing effect is due to the chemisorption of H_2S in the sorbent when placed in contact with H_2O and O_2. Indeed, H_2S molecules adsorbed at the surface undergo deprotonation by water forming HS^-, and consequently, reactions shown in Eq. (6) and Eq. (7) are expected to occur to a larger extent.

Contrarywise, the R7H sorbent exhibits the highest adsorption capacity at breakthrough under screening conditions, whilst oxygen reduces the adsorption capacity by 40%, and oxygen and relative humidity decrease the material performance by 70%. Indeed, the preferential adsorption of water, due to the higher affinity of water for the metal oxide surface compared to H_2S, is expected to saturate the adsorption sites, reducing the adsorption capacity of this material for H_2S.

Discussions

The results of the adsorption tests reported in the sections above show that the most efficient sorbent and the best operating conditions are different for the two contaminants studied, H_2S and COS.

A summary of the adsorption capacities against the two tested contaminants is shown in Table 13, both for dry and wet gas conditions.

H_2S Removal

For the most abundant contaminant in biogas, H_2S, the suitable sorbents under wet and dry conditions are activated carbon RGM3 and metal oxide R7H, respectively. The R7H material exhibits the best performance among the tested sorbents in contact with a dry biogas mixture without oxygen. However, the typical biogas composition contains traces of oxygen and moisture, which can be removed by cooling pre-treatments, but this requires more complex and expensive purification systems. Comparing the results with data from the literature is challenging because many parameters are involved in adsorption characterization, such as initial contaminant concentration, simulated biogas composition (CH_4, $CH_4 + CO_2$ or N_2 gas matrix, presence of oxygen and/or moisture), GHSV, reactor size, sorbent properties (surface area, pore-volume, material functionalisation, pellet/powder shape), and breakthrough set point.

The best performing sorbents activated carbon RGM3 and the metal oxide R7H are both Cu-functionalized: RGM3 is impregnated with copper carbonate and copper hydroxide, while R7H has a homogeneous and regular texture with crystalline inclusions of copper and oxygen compounds such as $Cu(OH)_2$ (see . Table 5 and Section S.2 in the Supplementary Material). The results show that Cu-functionalisation is effective. The activated carbon Ultra DS-6 uptakes a lower amount of H_2S compared to RGM3, which could be attributed to the K-functionalisation of the sorbent Ultra DS-6.

In the case of H_2S, the presence of moisture on certain groups of functionalized carbon increases their adsorption capacity, as reported by Cimino et al. [40], who investigate the adsorption capacity of H_2S on an activated carbon containing CuO and ZnO dispersions with different gas streams (N_2) containing either O_2 (2500 ppm_v), H_2O (50% RH) or O_2/H_2O at room temperature in a laboratory-scale fixed-bed reactor. The H_2S inlet concentration is 100 ppm_v. The results show that oxygen and water increase the H_2S adsorption capacity, especially for Cu-containing sorbents, and promote the formation of various sulphur species such as sulphides, sulphates and elemental sulphur. The saturation adsorption capacity of the activated carbon functionalized with CuO only is 2.99%g_{H2S}/g_{sorb} under screening conditions (anhydrous and anaerobic) and increases to 4.11 and 4.76%g_{H2S}/g_{sorb} in the presence of O_2 and H_2O, respectively. The simultaneous presence of O_2 and H_2O increases the performance of the material up to 12.9%g_{H2S}/g_{sorb}. The introduction of ZnO dispersion improves the adsorption performance under all conditions except in the co-presence of O_2 and H_2O. These results are consistent with those obtained in our adsorption tests on RGM3.

Cepollaro et al. [31] also tested a series of catalytic sorbents for the removal of H_2S (100 ppm_v inlet concentration) in a gas matrix of N_2 at low temperature and in the presence of oxygen (2500 ppm_v) and humidity (50% RH). The GHSV was 25,500 h^{-1} and the breakthrough was 5% of the inlet concentration. The materials studied were activated carbons functionalized with CuO, MgO and their combination. The H_2S adsorption capacity at breakthrough is 2.19 and 8.29%g_{H2S}/g_{sorb} for Cu-and Mg-based activated carbons, respectively. Under saturation conditions, the performance

is increased up to 22.2%g_{H2S}/g_{sorb} (Cu-based AC) and 24.2%g_{H2S}/g_{sorb}(Mg-based AC).

Wang et al. [41] investigated the performance of commercial adsorbents, including R7 and R8, to remove H_2S from simulated biogas containing 200 ppm_v H_2S, 10% N_2, 40% CO_2, and 50% CH_4. The SulfaTrap R7 sorbent was found to perform best at room temperature. The breakthrough capacity (H_2S concentration at outlet below 100 ppb) of R7 is 3.89%g_{H2S}/g_{sorb}. These results are comparable to those obtained in our experimental tests.

The rule of Cu-functionalisation for H_2S uptake has been reported in several papers, e.g., by Sisani et al. [42]. Barelli et al. [43]. Sisani compared the adsorption capacity of different sorbent materials, including the activated carbons RGM1 and Ultra DS. The materials were tested under dry conditions at room temperature, the inlet contaminant concentration was 200 ppm_v, and the GHSV was 10,000 h^{-1}. As in our work, the Cu-functionalized material (RGM1) is more efficient than K-based activated carbon (AC RBAA1 and Ultra DS). Moreover, the adsorption capacity of RBAA1 is higher than that of Ultra DS, which is due to the higher KOH content in the RBAA1 AC. The adsorption capacity at breakthrough (last detection of 0 ppm_v) is 2.72%g_{H2S}/g_{sorb}, 2.04%g_{H2S}/g_{sorb} and 0.66%g_{H2S}/g_{sorb} for RGM1, RBAA1, and Ultra DS, respectively. RGM1 and Ultra DS sorbents have also been tested under humid conditions (RH = 50%). The performance of the RGM1 sample were only slightly enhanced (+ 2%), while Ultra DS shows a significant increase of H_2S uptake (+ 210%).

Barelli, also compared the performance of the activated carbons Norit RGM1 and Ultra DS. The gas matrix is N_2 or $CH_4 + CO_2$ with 2%$_{vol}$ O_2, 0–90% RH, and 100 ppm_v H_2S. Under dry conditions, the adsorption capacity of RGM1 (2.58%g_{H2S}/g_{sorb}) is more than 60% higher than that of Airpel Ultra DS (1.57%g_{H2S}/g_{sorb}). The performance of Airpel Ultra DS is enhanced by humidity (2.61%g_{H2S}/g_{sorb} at 50% RH and 3.48%g_{H2S}/g_{sorb} at 90% RH) which is due to the formation of a water film around the activated carbon pores, that favours the dissociation of H_2S molecules.

Other similar results for the removal of H_2S are reported in [44–48] for Cu-functionalized activated carbons, in [49–51] for K-functionalized activated carbons, and in [45, 52, 53] for metal oxides.

COS Removal

The R8C sorbent has been specifically optimized by Sulfatrap for the removal of COS. It is therefore surprising that its performance in COS uptaking was not better than that of other ACs: the reason is that the operating conditions required for effective removal of COS are far from our screening conditions, both in terms of temperature and humidity [15].

Dedicated tests were performed on the most performant sorbent in screening conditions, RGM3, to check its behavior under different COS concentrations.

The effect of inlet COS concentration on the dynamic adsorption process is significant; the adsorption capacity decreases with reducing the COS partial pressure in the gas stream. The decrease of activated carbons adsorption capacity with contaminant partial pressure is a general result, independent from the contaminant [54]. Similar behavior was also stated for H_2S in the studies of Xiao and Wang [55]. As explained in the Xiao's work it is probably due to minor interaction between the sorbent and the contaminant, in fact, for lower feed concentrations, a lower mass-transfer flux is achieved from the bulk gas to the particle surface, due to the decreased driving force. On the other hand, higher feed concentration yields enhance driving force along with the pores, resulting in steeper breakthrough curves and faster equilibrium.

Interesting results were obtained during the campaign under dry conditions. In particular, for COS, the adsorption capacity of the ACs shows no trend correlated with their surface areas, differently from what is shown in presence of humidity. The best performance under dry conditions is obtained with Ultra DS-6 and R8C, namely 1.88% and 2.4% g of COS per gramme of sorbent, respectively. A possible explanation for the better results of these two sorbents compared to RGM3, which has a larger surface area, can be found in the impregnated compounds. As shown in the EDX and EDS results (Figure S12 and S14 in the Supplementary Material), Ultra DS-6 and R8C exhibit a large amount of potassium on their surface, suggesting potassium hydroxide-K(OH) or potassium oxide-K_2O as impregnated candidates. Indeed, these compounds could interact weakly with COS to enhance C_{ads}. A chemical reaction between the sorbents and COS is excluded on the basis of the desorption test carried on after adsorption tests, which show that no chemical reactions take place during these tests, only weak intermolecular forces (Van der Waals forces, dipole–dipole interaction, etc.).

To explain the low performance of COS removal in presence of water, we suppose possible competition between water and COS on physisorption sites on the ACs surface. Our results show a much more pronounced effect on some sorbents (DS-6 and R8C) than on others. We ascribe this to the DS-6 and R8C functionalization with potassium as shown in Table 5 and Supplementary material. In humid conditions water molecules compete with COS ones in occupying the pore sites. The competition between the CO_2 and COS diluted in the water film can contribute to explain the obtained results, as CO_2 and COS dissolve in the same way in water but the partial pressure of CO_2 is orders of magnitude larger than that of COS.

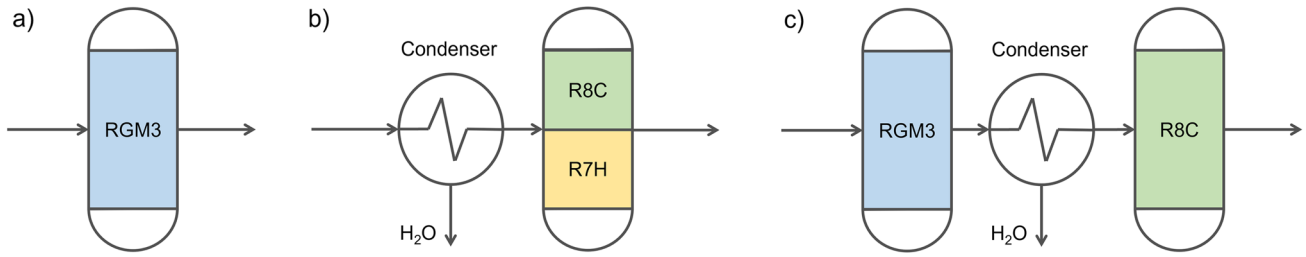


Fig. 16 Schematic of the plant configurations for sulphur compounds removal: **a** wet gas and single-vessel configuration; **b** dry gas and single-vessel configuration; **c** two-vessel configuration with intermediate drying

As explained in the experimental studies conducted by Jonas et al. [56], the reduction in adsorbing capacity depends on the solubility of the gases in water. For gases that are soluble in water and subsequently hydrolysed by it, the adsorption phenomena should be enhanced with increasing humidity. For gases that are soluble in water but are not hydrolyzed by it, there should be no effect on adsorption. For gases that are not soluble in water, the adsorption capacity should be reduced. The low solubility of COS is the reason for the reduced capacity of every sorbent in the presence of a humid biogas stream. The influence of relative humidity (RH) on the adsorption of COS was also investigated by Sattler and Rosenberk [57] in 2006. The experimental results showed that the adsorption capacity of COS on various AC sorbents decreased with increasing humidity. It was concluded that COS is not sufficiently soluble in water to enhance adsorption capacity under humid conditions. The same result was obtained by Hernandez, Solarino et al. [58] in their work on the desulphurization process of natural gas for fuel cell systems. Again, the presence of water vapor significantly reduces both the selectivity and the uptake capacity toward sulphur compounds.

Simultaneous H_2S and COS Removal

The only work on contemporary uptake of H_2S and COS is the very recent work by Li et al. [59]. The GHSV was 30,000 h^{-1}, the reactor temperature 60 °C and the breakthrough point was defined as the point at which the contaminant concentration at the outlet was 10% of the concentration at the inlet. Under these conditions, the adsorption capacity achieved is 9.06%g_{COS}/g_{sorb} and 12.76%g_{H2S}/g_{sorb} for COS and H_2S removal, respectively. The adsorption capacity of COS is an order of magnitude higher than the capacity calculated in our analysis at saturation of RGM3 (Cu-functionalisation) and Ultra DS-6 (K-functionalisation). This is due to the different operating conditions, especially temperature: from room temperature to 60 °C, the removal efficiency of AC increases considerably. The data obtained in this article (summarized in Table 13) can be used to design an optimal configuration of reactors for the biogas purification system. Working under real conditions, i.e. in the presence of wet biogas, with a single reactor and a single sorbent that can remove both impurities would be ideal. However, although RGM3 has proven effective in removing both contaminants, its low adsorption capacity, especially for COS, could cause several problems both from an operational (replacement of the sorbent) and economic (maintenance costs) point of view. For this reason, we propose three possible solutions (Fig. 16) for the design of the biogas purification system:

(i) Single-vessel configuration and wet gas (Fig. 16a). This is the simplest solution, where a single vessel (filled with RGM3) is fed directly with the wet biogas (non-condensing). It represents the lowest complexity in terms of plant design, but has low removal efficiency, especially regarding COS.
(ii) Single-vessel configuration and dry gas (Fig. 16b). This solution involves biogas preconditioning through a condenser to reduce its relative humidity. The dry gas is then fed into the single vessel reactor, which is partly filled with R7H for H_2S removal and partly with R8C for COS removal. This is an intermediate solution in terms of plant complexity and shows good efficiency for both contaminants.
(iii) Two-vessel configuration with intermediate drying (Fig. 16c). Two reactors filled with RGM3 and R8C respectively; the humid (non-condensing) biogas goes directly into the first reactor for H_2S removal, then a condenser reduces the relative humidity for COS uptake in the second reactor. This is the more complex design but offers the highest efficiency among the three proposed solutions.

The optimal of the three proposed solutions should be examined from time to time, considering the system size, biogas quality, space requirements and the costs of installing the condenser.

An example of a plant with a two-vessel configuration is reported by Calbry-Muzyka et al. [60], who tested an adsorption-based cleaning unit for the deep desulphurisation

of biogas in a pilot plant (COSYMA project). The H_2S is adsorbed to the metal oxide sorbent R7 in the first stage, while the other impurities (COS, DMS, terpenes, siloxanes) are by the sorbents R8 and R2 in the second stage.

Conclusions

In the framework of the European project Waste2Watts, the performances of commercial sorbents were characterized using different techniques and their removal capacities were tested. The removal efficiency towards H_2S and COS was investigated under certain conditions. The experimental activity investigated the possibility to find sorbents for the combined removal of pollutants such as H_2S and COS. The final objective is to find a viable solution for the development of a flexible and cost-effective purification unit for the removal of impurities for biogas utilization in solid oxide fuel cell systems. Starting from a reference experimental set-up, the effects of oxygen, humidity and contaminant inlet concentration on the sorbents' performance have been investigated. Even if each contaminant requires a different sorbent depending on the operative conditions, good performance is achieved by RGM3 for the combined removal of H_2S and COS in humid (50%RH) conditions. In case of dry biogas, R7H for is the best choice for H_2S and R8C the one for COS. Water can be removed by introducing a cooling system between the digester and the sorbents, although this solution implies higher complexity and cost for the purification unit, especially for small size plants.

The aim of this work is to analyse the sorbents performance in different gas matrixes and finding a compromise, accepting some capacity lowering in exchange for a simple and economic clean-up layout (single reactor). Therefore, based on the experimental results, the authors propose three possible plant configurations to take advantage of the properties of the sorbents and aimed to remove both H_2S and COS: (i) a single vessel with RGM3 for both H_2S and COS removal without biogas pre-conditioning chiller; (ii) a single vessel after the conditioning unit filled with R7H for H_2S removal and R8C for COS removal, and (iii) two vessels with intermediate drying with RGM3 for H_2S uptake in humid conditions and R8C for COS removal from the dry gas.

The convenience of each solution should be evaluated time by time considering the biogas quality, the space concerns, and the cost and opportunity to insert the condenser. A detailed cost-optimal evaluation of the clean-up system sizing based on the project's experimental data will be the object of subsequent authors' work.

Supplementary Information The online version contains supplementary material available at https://doi.org/10.1007/s12649-023-02212-6.

Funding Open access funding provided by Ente per le Nuove Tecnologie, l'Energia e l'Ambiente within the CRUI-CARE Agreement. The study has been done in the framework of the Waste2Watts project (Grant Agreement n. 826234) supported by the Clean Hydrogen Partnership and its members, Hydrogen Europe and Hydrogen Europe Research.

Data Availability Enquiries about data availability should be directed to the authors.

Declarations

Competing interests The authors have not disclosed any competing interests.

Open Access This article is licensed under a Creative Commons Attribution 4.0 International License, which permits use, sharing, adaptation, distribution and reproduction in any medium or format, as long as you give appropriate credit to the original author(s) and the source, provide a link to the Creative Commons licence, and indicate if changes were made. The images or other third party material in this article are included in the article's Creative Commons licence, unless indicated otherwise in a credit line to the material. If material is not included in the article's Creative Commons licence and your intended use is not permitted by statutory regulation or exceeds the permitted use, you will need to obtain permission directly from the copyright holder. To view a copy of this licence, visit http://creativecommons.org/licenses/by/4.0/.

References

1. IRENA - International Renewable Energy Agency: Renewable energy statistics 2021. IRENA, Masdar City (2021)
2. EBA: Statistical report of the European biogas association 2021. EBA, Brussels (2021)
3. Kampman, B., Leguijt, C., Scholten, T., Tallat-Kelpsaite, J., Brückmann, R., Maroulis, G., Lesschen, J.P., Meesters, K., Sikirica, N., Elbersen, B.: Optimal use of biogas from waste streams. An assessment of the potential of biogas from digestion in the EU beyond 2020. (2016). https://doi.org/10.13140/RG.2.2.14770.40643
4. Banja, M., Jégard, M., Motola, V., Sikkema, R.: Support for biogas in the EU electricity sector—a comparative analysis. Biomass Bioenergy **128**, 105313 (2019). https://doi.org/10.1016/J.BIOMBIOE.2019.105313
5. Scarlat, N., Dallemand, J.F., Fahl, F.: Biogas: developments and perspectives in Europe. Renew. Energy **129**, 457–472 (2018). https://doi.org/10.1016/j.renene.2018.03.006
6. Giarola, S., Forte, O., Lanzini, A., Gandiglio, M., Santarelli, M., Hawkes, A.: Techno-economic assessment of biogas-fed solid oxide fuel cell combined heat and power system at industrial scale. Appl. Energy **211**, 689–704 (2018). https://doi.org/10.1016/j.apenergy.2017.11.029
7. Oluleye, G., Gandiglio, M., Santarelli, M., Hawkes, A.: Pathways to commercialisation of biogas fuelled solid oxide fuel cells in European wastewater treatment plants. Appl. Energy **282**, 116127 (2021). https://doi.org/10.1016/j.apenergy.2020.116127
8. Lanzini, A., Madi, H., Chiodo, V., Papurello, D., Maisano, S., Santarelli, M., Van herle, J.: Dealing with fuel contaminants in biogas-fed solid oxide fuel cell (SOFC) and molten carbonate fuel cell (MCFC) plants: degradation of catalytic and electro-catalytic active surfaces and related gas purification methods. Prog. Energy

Combust. Sci. **61**, 150–188 (2017). https://doi.org/10.1016/j.pecs.2017.04.002
9. Hassanzadeh, H., Mansouri, S.H.: Efficiency of ideal fuel cell and Carnot cycle from a fundamental perspective. Proc. IMechE Part A: J. Power Energy (2005). https://doi.org/10.1243/095765005X28571
10. Gandiglio, M., Lanzini, A., Santarelli, M., Acri, M., Hakala, T., Rautanen, M.: Results from an industrial size biogas-fed SOFC plant (the DEMOSOFC project). Int. J. Hydrogen Energy **45**, 5449–5464 (2020). https://doi.org/10.1016/j.ijhydene.2019.08.022
11. Langnickel, H., Rautanen, M., Gandiglio, M., Santarelli, M., Hakala, T., Acri, M., Kiviaho, J.: Efficiency analysis of 50 kWe SOFC systems fueled with biogas from waste water. J. Power Sources Adv. **2**, 100009 (2020). https://doi.org/10.1016/j.powera.2020.100009
12. Gandiglio, M.: Design and operation of an industrial size adsorption-based cleaning system for biogas use in fuel cells. Energy **259**, 124941 (2022). https://doi.org/10.1016/J.ENERGY.2022.124941
13. Saadabadi, S.A., Thallam Thattai, A., Fan, L., Lindeboom, R.E.F., Spanjers, H., Aravind, P.V.: Solid oxide fuel cells fuelled with biogas: potential and constraints. Renew. Energy (2019). https://doi.org/10.1016/j.renene.2018.11.028
14. Mermelstein, J., Posdziech, O.: Development and demonstration of a novel reversible SOFC system for utility and micro grid energy storage. Fuel Cells **17**, 562–570 (2017). https://doi.org/10.1002/FUCE.201600185
15. Sitthikhankaew, R., Chadwick, D., Assabumrungrat, S., Laosiripojana, N.: Effects of humidity, O2, and CO2 on H2S adsorption onto upgraded and KOH impregnated activated carbons. Fuel Process. Technol. **124**, 249–257 (2014). https://doi.org/10.1016/j.fuproc.2014.03.010
16. Calbry-Muzyka, A., Madi, H., Rüsch-Pfund, F., Gandiglio, M., Biollaz, S.: Biogas composition from agricultural sources and organic fraction of municipal solid waste. Renew. Energy **181**, 1000–1007 (2022). https://doi.org/10.1016/J.RENENE.2021.09.100
17. Lackey, J., Champagne, P., Peppley, B.: Use of wastewater treatment plant biogas for the operation of Solid Oxide Fuel Cells (SOFCs). J. Environ. Manage. (2016). https://doi.org/10.1016/j.jenvman.2016.09.006
18. Becker, C.M., Marder, M., Junges, E., Konrad, O.: Technologies for biogas desulfurization—an overview of recent studies. Renew. Sustain. Energy Rev. **159**, 112205 (2022). https://doi.org/10.1016/J.RSER.2022.112205
19. Paglini, R., Gandiglio, M., Lanzini, A.: Technologies for deep biogas purification and use in zero-emission fuel cells systems. Energies **15**, 3551 (2022). https://doi.org/10.3390/EN15103551
20. Papurello, D., Gandiglio, M., Lanzini, A.: Experimental analysis and model validation on the performance of impregnated activated carbons for the removal of hydrogen Sulfide (H2S) from sewage biogas. Processes **7**, 548 (2019). https://doi.org/10.3390/pr7090548
21. Micoli, L., Bagnasco, G., Turco, M.: H2S removal from biogas for fuelling MCFCs: New adsorbing materials. Int. J. Hydrogen Energy **39**, 1783–1787 (2014). https://doi.org/10.1016/J.IJHYDENE.2013.10.126
22. Papurello, D., Silvestri, S., Lanzini, A.: Biogas cleaning: trace compounds removal with model validation. Sep. Purif. Technol. **210**, 80–92 (2019). https://doi.org/10.1016/j.seppur.2018.07.081
23. Calbry-Muzyka, A.S., Schildhauer, T.J.: Direct methanation of biogas—technical challenges and recent progress. Front. Energy Res. **8**, 356 (2020). https://doi.org/10.3389/FENRG.2020.570887/BIBTEX
24. Wasajja, H., Lindeboom, R.E.F., van Lier, J.B., Aravind, P.V.: Techno-economic review of biogas cleaning technologies for small scale off-grid solid oxide fuel cell applications. Fuel Process. Technol. **197**, 106215 (2020). https://doi.org/10.1016/J.FUPROC.2019.106215
25. Ghimire, A., Gyawali, R., Lens, P.N.L., Lohani, S.P.: Technologies for removal of hydrogen sulfide (H2S) from biogas. Emerg. Technol. Biol. Syst. Biogas Upgrad. (2021). https://doi.org/10.1016/B978-0-12-822808-1.00011-8
26. Awe, O.W., Zhao, Y., Nzihou, A., Minh, D.P., Lyczko, N.: A review of biogas utilisation, purification and upgrading technologies. Waste Biomass Valorization **8**, 267–283 (2017). https://doi.org/10.1007/S12649-016-9826-4/FIGURES/9
27. National Center for Biotechnology Information: Carbonyl sulfide | COS – PubChem. https://pubchem.ncbi.nlm.nih.gov/compound/Carbonyl-sulfide
28. Bahadori, A.: Natural gas sweetening. Natural gas processing, pp. 483–518. Elsevier, Amsterdam (2014). https://doi.org/10.1016/B978-0-08-099971-5.00010-6
29. Kohl, A.L., Nielsen, R.: Gas purification. Gulf Pub, Houston (1997)
30. Sherman, J.D., Katsaros, A.T.: Patent US4329160A - Suppression of COS formation in molecular sieve purification of hydrocarbon gas streams, 1978
31. Cepollaro, E.M., Caputo, D., Gargiulo, N., Deorsola, F.A., Cimino, S., Lisi, L.: H2S catalytic removal at low temperature over Cu- and Mg- activated carbon honeycombs. Catal Today (2021). https://doi.org/10.1016/j.cattod.2021.11.027
32. Waste2watts-project, https://waste2watts-project.net/
33. Gandiglio, M., Lanzini, A., Santoni, F., Gislon, P., Aurora, A., Della Seta, L., Mcphail, S.J., Biollaz, S.M.A., Schildhauer, T.J., Wieseler, T., Indlekofer, J., Madi, H., Calbry-Muzyka, A.S.: Sorbent testing intermediate report. Deliverable D2.3. Waste2Watt EU Project. (2020)
34. Sitthikhankaew, R., Chadwick, D., Assabumrungrat, S., Laosiripojana, N.: Effects of humidity, O2, and CO2 on H2S adsorption onto upgraded and KOH impregnated activated carbons. Fuel Process. Technol. (2014). https://doi.org/10.1016/j.fuproc.2014.03.010
35. Li, Y., Lin, Y., Xu, Z., Wang, B., Zhu, T.: Oxidation mechanisms of H2S by oxygen and oxygen-containing functional groups on activated carbon. Fuel Process. Technol. **189**, 110–119 (2019). https://doi.org/10.1016/j.fuproc.2019.03.006
36. Yan, R., Liang, D.T., Tsen, L., Tay, J.H.: Kinetics and mechanisms of H2S adsorption by alkaline activated carbon. Environ. Sci. Technol. **36**, 4460–4466 (2002). https://doi.org/10.1021/ES020584O/SUPPL_FILE/ES0205840_S.PDF
37. Wesley Awe, O., Zhao, Y., Nzihou, A., Pham Minh, D., Lyczko, N.: A review of biogas utilisation purification and upgrading technologies. Waste Biomass Valorization **8**, 267–283 (2017). https://doi.org/10.1007/s12649-016-9826-4ï
38. Thommes, M., Kaneko, K., Neimark, A.V., Olivier, J.P., Rodriguez-Reinoso, F., Rouquerol, J., Sing, K.S.W.: Physisorption of gases, with special reference to the evaluation of surface area and pore size distribution (IUPAC Technical Report). Pure Appl. Chem. **87**, 1051–1069 (2015). https://doi.org/10.1515/pac-2014-1117
39. Raabe, T., Mehne, M., Rasser, H., Krause, H., Kureti, S.: Study on iron-based adsorbents for alternating removal of H2S and O2 from natural gas and biogas. Chem. Eng. J. **371**, 738–749 (2019). https://doi.org/10.1016/j.cej.2019.04.103
40. Cimino, S., Lisi, L., Erto, A., Deorsola, F.A., de Falco, G., Montagnaro, F., Balsamo, M.: Role of H2O and O2 during the reactive adsorption of H2S on CuO-ZnO/activated carbon at low temperature. Microporous Mesoporous Mater. **295**, 109949 (2020). https://doi.org/10.1016/J.MICROMESO.2019.109949
41. Wang, X., Quan, W., Xiao, J., Peduzzi, E., Fujii, M., Sun, F.: Solid oxide fuel cells operating on alternative and renewable fuels - Final technical report - DOE Cooperative Agreement No. DE-NT0004396. (2014)

42. Sisani, E., Cinti, G., Discepoli, G., Penchini, D., Desideri, U., Marmottini, F.: Adsorptive removal of H2S in biogas conditions for high temperature fuel cell systems. Int. J. Hydrogen Energy **39**, 21753–21766 (2014). https://doi.org/10.1016/j.ijhydene.2014.07.173
43. Barelli, L., Bidini, G., de Arespacochaga, N., Pérez, L., Sisani, E.: Biogas use in high temperature fuel cells: enhancement of KOH-KI activated carbon performance toward H2S removal. Int. J. Hydrogen Energy **42**, 10341–10353 (2017). https://doi.org/10.1016/j.ijhydene.2017.02.021
44. Chen, S., Guo, Y., Zhang, J., Guo, Y., Liang, X.: CuFe2O4/activated carbon adsorbents enhance H2S adsorption and catalytic oxidation from humidified air at room temperature. Chem. Eng. J. **431**, 134097 (2022). https://doi.org/10.1016/J.CEJ.2021.134097
45. Wang, J., Wang, L., Fan, H., Wang, H., Hu, Y., Wang, Z.: Highly porous copper oxide sorbent for H 2 S capture at ambient temperature. Fuel **209**, 329–338 (2017). https://doi.org/10.1016/j.fuel.2017.08.003
46. Golmakani, A., Ali Nabavi, S., Wadi, B., Manovic, V.: Advances, challenges, and perspectives of biogas cleaning, upgrading, and utilisation. Fuel **317**, 123085 (2022). https://doi.org/10.1016/J.FUEL.2021.123085
47. Huang, C.C., Chen, C.H., Chu, S.M.: Effect of moisture on H2S adsorption by copper impregnated activated carbon. J. Hazard. Mater. **136**, 866–873 (2006). https://doi.org/10.1016/j.jhazmat.2006.01.025
48. de Falco, G., Montagnaro, F., Balsamo, M., Erto, A., Deorsola, F.A., Lisi, L., Cimino, S.: Synergic effect of Zn and Cu oxides dispersed on activated carbon during reactive adsorption of H2S at room temperature. Microporous Mesoporous Mater. **257**, 135–146 (2018). https://doi.org/10.1016/J.MICROMESO.2017.08.025
49. Frilund, C., Hiltunen, I., Simell, P.: Activated carbons for syngas desulfurization: evaluating approaches for enhancing low-temperature H2S oxidation rate. ChemEng. **5**, 23 (2021). https://doi.org/10.3390/CHEMENGINEERING5020023
50. Sitthikhankaew, R., Predapitakkun, S., Kiattikomol, R., Pumhiran, S., Assabumrungrat, S., Laosiripojana, N.: Comparative study of hydrogen sulfide adsorption by using alkaline impregnated activated carbons for hot fuel gas purification. Energy Procedia **9**, 15–24 (2011). https://doi.org/10.1016/J.EGYPRO.2011.09.003
51. Zeng, F., Liao, X., Hu, H., Liao, L.: Effect of potassium hydroxide activation in the desulfurization process of activated carbon prepared by sewage sludge and corn straw. J. Air. Waste Manage. Assoc. **68**, 255–264 (2018). https://doi.org/10.1080/10962247.2017.1407378
52. Georgiadis, A.G., Charisiou, N.D., Goula, M.A.: Removal of hydrogen sulfide from various industrial gases: a review of the most promising adsorbing materials. Catalysts **10**, 521 (2020). https://doi.org/10.3390/CATAL10050521
53. Costa, C., Cornacchia, M., Pagliero, M., Fabiano, B., Vocciante, M., Reverberi, A.P.: Hydrogen sulfide adsorption by iron oxides and their polymer composites: a case-study application to biogas purification. Materials **13**, 4725 (2020). https://doi.org/10.3390/MA13214725
54. Keller, J.U., Staudt, R.: Adsorption isotherms. In: gas adsorption equilibria, pp. 359–413. Springer, Boston (2005)
55. Xiao, Y., Wang, S., Wu, D., Yuan, Q.: Experimental and simulation study of hydrogen sulfide adsorption on impregnated activated carbon under anaerobic conditions. J. Hazard. Mater. **153**, 1193–1200 (2008). https://doi.org/10.1016/j.jhazmat.2007.09.081
56. Jonas, L.A., Sansone, E.B., Farris, T.S.: The effect of moisture on the adsorption of chloroform by activated CarbonA. Am. Ind. Hyg. Assoc. J. **46**, 20–23 (1985). https://doi.org/10.1080/15298668591394310
57. Sattler, M.L., Rosenberk, R.S.: Removal of carbonyl sulfide using activated carbon adsorption. J. Air Waste. Manage. Assoc. **56**, 219–224 (2006). https://doi.org/10.1080/10473289.2006.10464450
58. Hernández, S., Solarino, L., Orsello, G., Russo, N., Fino, D., Saracco, G., Specchia, V.: Desulfurization processes for fuel cells systems. Int. J. Hydrogen Energy. **33**, 3209–3214 (2008). https://doi.org/10.1016/j.ijhydene.2008.01.047
59. Li, X., Wang, X., Wang, L., Ning, P., Ma, Y., Zhong, L., Wu, Y., Yuan, L.: Efficient removal of carbonyl sulfur and hydrogen sulfide from blast furnace gas by one-step catalytic process with modified activated carbon. Appl. Surf. Sci. (2022). https://doi.org/10.1016/j.apsusc.2021.152189
60. Calbry-Muzyka, A.S., Gantenbein, A., Schneebeli, J., Frei, A., Knorpp, A.J., Schildhauer, T.J., Biollaz, S.M.A.: Deep removal of sulfur and trace organic compounds from biogas to protect a catalytic methanation reactor. Chem. Eng. J. **360**, 577–590 (2019). https://doi.org/10.1016/j.cej.2018.12.012

Publisher's Note Springer Nature remains neutral with regard to jurisdictional claims in published maps and institutional affiliations.

Authors and Affiliations

F. Santoni[1] · P. Gislon[1] · E. Rozzi[2] · M. Gandiglio[2] · S. McPhail[1] · A. Lanzini[2] · M. Pagani[3] · S. Fiorilli[3]

✉ F. Santoni
francesca.santoni@enea.it

[1] Laboratory of Storage, Battery and Hydrogen Production & Use, Department of Energy Technologies and Renewable Sources (TERIN-PSU-ABI), ENEA, C.R. Casaccia, Via Anguillarese 301, 00123 Rome, Italy

[2] Department of Energy, Politecnico Di Torino, C.So Duca Degli Abruzzi 24, 10129 Turin, Italy

[3] Department of Applied Science and Tehcnology, Politecnico Di Torino, C.So Duca Degli Abruzzi 24, 10129 Turin, Italy